SYNTHESIS AND AGGLOMERATION OF GOLD NANOPARTICLES IN REVERSE MICELLES

By
Adriana Patricia Herrera Barros

A thesis submitted in partial fulfillment of the requirements for the degree of

MASTER OF SCIENCE
In
CHEMICAL ENGINEERING

UNIVERSITY OF PUERTO RICO

MAYAGÜEZ CAMPUS

2005

Approved by:

_____	_____
Carlos Rinaldi, PhD President, Graduate Committee	Date
_____	_____
Julio G Briano, PhD Member, Graduate Committee	Date
_____	_____
Miguel Castro, PhD Member, Graduate Committee	Date
_____	_____
Nelson Cardona Martinez, PhD Department Chair	Date

ABSTRACT

Reverse micelles prepared in the system water, sodium bis-(2-ethylhexyl) sulfoccinate (AOT), and isooctane were investigated as a templating system for the production of gold nanoparticles from the reduction of Au (III) by sulfite ions. A core-shell Mie model was used to describe the optical properties of gold nanoparticles synthesized inside the reverse micelles. Dynamic light scattering measurements of gold colloids in aqueous media and in reverse micelle solution indicated agglomeration of micelles containing particles. This agglomeration was verified theoretically by estimating the total interaction energy between pairs of particles as a function of particle size. The analysis indicated that particles larger than about 8 nm diameter should reversibly flocculate. Transmission Electron Microscopy measurements of gold nanoparticles produced inside reverse micelles showed diameters of 8 to 10 nm. Evidence of cluster formation was also observed. Time correlated UV-Vis absorption measurements showed a red shift for the peak wavelength. This was interpreted as the result of multiple scattering and plasmon interaction between particles due to agglomeration of micelles with particles larger than 8 nm.

ACKNOWLEDGMENTS

Three years ago nanotechnology seemed to me as an exotic word that grouped the futurist inclination of the scientific community. Today, this word represents to me more than a field of research in which I can develop my scientific criteria; it is as a window that allows me to see inside a beaker a whole universe of atomic dimensions with amazing properties.

I would like to thank everyone who helped me make this work possible; specially my advisor Dr. Carlos Rinaldi for his friendship, and for teaching me a new concept of science research. His advice guided the ideas that allowed me to achieve the proposed goals of this investigation. My deepest gratitude to Drs. Julio Briano and Miguel Castro, members of my graduate committee for their guidance and collaboration in the development of this work. I will also like to thank the University of Puerto Rico, Mayagüez Campus, and the Chemical Engineering Department, for allowing me the opportunity to do my Master of Science degree. Special mention to the Center for Nanoscale Materials of the UPR-Río Piedras for the use of High Resolution Transmission Electron Microscope, and Mr. Oscar Resto for skillfully helping with these measurements. NSF and the Puerto Rico NSF-EPSCoR for supporting this work.

I also wish to express my acknowledgment to my friend and doctoral candidate Eder Vicuña for his helpful comments and suggestions regarding Mie theory. My profound gratitude to the doctoral students, dear friends and partners in research: Victoria Calero,

Carola Barrera, and Arlex Chaves for helping me grow as a person, and sharing with me special moments in the lab.

Thanks from my heart to my family for their spiritual support. Richard my love, you are not only my husband and best friend, you are my soul mate, who let me reach a perfect balance in this chaotic world. My little son Ricardo Andres, you changed my life; your smile brings me the necessary strength to fight for our dreams. Any words are not sufficient to thank my parents Ramon and Denis; this triumph is yours. No distance could break the love ties that bind our hearts. Nayibe, Carmen, Guillermo, and Esther my dear brothers, thanks for giving me your love at the moments in which I most need it. Special people have been present in my way, among them Rafael Perez and Carlos Monge, thanks my friends for your prayers and company.

TABLE OF CONTENTS

LISTS OF FIGURES……..vi

LISTS OF TABLES…….viii

1. INTRODUCTION AND BACKGROUND……1

1.1 Introduction……..……..……..……..1

1.2 Background……..……..…3

1.2.1 Reverse Micelles….……..……3

1.2.2 Mie Theory.……..……..…..16

2. PREVIOUS WORK……....……..23

2.1 Synthesis and growth of gold nanoparticles in aqueous media..……..……...23

2.2 Synthesis of gold nanoparticles using reverse micelles….……..……24

3. MATERIALS AND METHODS…….……...……...26

3.1 Reactants……...……..……..……...26

3.2 Determination of reverse micelle size…….…….……27

3.3 Preparation of reverse micelles……..……..29

3.4 Gold nanoparticle synthesis……..……...30

3.5 Gold colloids in aqueous media……..…….31

3.6 Characterization……..…….31

4. RESULTS AND DISSCUSSION…..……...…...……...……...33

4.1 Extinction measurements ……..……...……...33

4.2 Dynamic Light Scattering (DLS) measurements……..……...36

4.3 Particle-Particle interaction in reverse micelles……..…….38

4.4 Transmission Electron Microscope (TEM) measurements……..……42

4.5 Growth and agglomeration kinetics……..……...43

5. CONCLUSIONS ……..……...…….…….……...46

6. RECOMMENDATIONS…..……...…….……...……..……...48

APPENDIX A

Collision parameters for reverse micelles with *w* = 10……...……...……...51

A.1 Collision rate (Z)…….....51

A.2 Time between collisions (t)…….....53

APPENDIX B

Calculation of the solubility parameters of AOT in Isooctane…..…..……...……..…….54

B.1 AOT Solubility (δ_2)…….....54

B.2 Flory Huggins parameter (χ)……...55

APPENDIX C

Volumetric fraction (ϕ_{vol}) of gold colloid standards in aqueous media and in water/AOT/isooctane solution……...56

APPENDIX D

Calculation of the theoretical yield and volumetric fraction of gold nanoparticles synthesized in reverse micelles with *w* = 10……...……...…….....57

D.1 Theoretical yield…….57

D.2 Volumetric fractions……...58

APPENDIX E

Change in the peak extinction wavelength during reaction time…..……...…….59

BIBLIOGRAPHY……62

LIST OF FIGURES

Figure 1: Comparison of sizes of two nano-structures: A) biological configuration of a virus and, B) carbon nano-wire arrangement……...……...1

Figure 2: Use of gold nanoparticle as tag to promote DNA dehybridization process...…..2

Figure 3: Conceptual illustration of a reverse micelle system……...……..3

Figure 4: Illustration of micellar morphologies: reverse micelle (A), normal micelle (B) interconnected cylinders (C), planar lamellar phase (D)…….....4

Figure 5: Principal forces acting on a reverse micelle……...……..5

Figure 6: Structure of Aerosol OT. Carbon molecules are represented by grey spheres, oxygen molecules by red spheres, and sulphur and sodium molecules by yellow and blue spheres respectively…….. 8

Figure 7: Illustration of the micellar exchange process…….....10

Figure 8: Representation of micellar association kinetics in a reverse micelle……12

Figure 9: Phase Diagram for AOT/Isooctane/Water ternary system at 298 K. Oil in water (O/W: micelles), water in oil (W/O: reverse micelles), and lamellar sheets……..16

Figure 10: Plasmon resonance phenomena……17

Figure 11: Energy transfer from the absorption of light by a spherical particle……18

Figure 12: Core shell spherical particle…….....23

Figure 13: Schematic representation of synthesis of gold nanoparticles in reverse micelle……..……24

Figure 14: Phase diagram for reverse micelle *w*=10: Aqueous/AOT/Isooctane……. .28

Figure 15: Conceptual illustration of reverse micelle structure……...……..28

Figure 16: Hydrodynamic diameter measurements for water/AOT/isooctane reverse micelles……..29

Figure 17: Gold nanoparticles synthesized in reverse micelles with *w* = 10……....31

Figure 18: Absorption measurements of gold colloid standards in aqueous medium…...34

Figure 19: Absorption of gold colloid standards in AOT/water/isooctane reverse micelles with w = 10……..34

Figure 20: Peak wavelength correlation with particle size for gold nanoparticle in reverse micelles with w = 10……....36

Figure 21:Comparison between nominal size of gold colloid standards and hydrodynamic diameter measured by DLS instrument. • gold colloid standards in aqueous medium, and Δ gold colloid standards in reverse micelles solution. The solid line represents exact correspondence between our measured hydrodynamic diameter and the value reported by the supplier……..37

Figure 22: Contributions to the total interaction energy for gold nanoparticles coated with a layer of AOT and immersed in isooctane at 25°C. Particle diameter is 6.4 nm……....41

Figure 23: Total interaction energy as a function of separation distance for various particle diameters…….....41

Figure 24: TEM of gold nanoparticles synthesized with Au3 concentration in w =10 reverse micelles…….…..42

Figure 25: Time correlated absorption spectra of gold nanoparticles synthesized in reverse micelles with w = 10 for Au1 sample concentration ($KAuCl_4$[38 mM], K_2SO_3[129.49 mM])……44

Figure 26: Change in the peak absorption wavelength with for gold nanoparticles synthesized in reverse micelles with w = 10 for: a) Au1: $KAuCl_4$ [38 mM], K_2SO_3 [129.49 mM], b) Au2: $KAuCl_4$ [57.55 mM], K_2SO_3 [194.24 mM], and c) Au3: $KAuCl_4$ [76.74 mM], K_2SO_3 [258.99 mM]……...45

Figure 27: Illustration of the measurement of forces between a gold coated tip and a gold flat substrate in AOT/Isooctane solution using an AFM…….50

Figure E-1: Au1 up to 262 s Au1: $KAuCl_4$ [38 mM], K_2SO_3 [129.49 mM].....59

Figure E-2: Au2 up to 262 s Au1: $KAuCl_4$ [57.55 mM], K_2SO_3 [194.24 mM]……60

Figure E-3: Au3 up to 262 s. Au1: $KAuCl_4$ [76.74 mM], K_2SO_3 [258.99mM].....61

LIST OF TABLES

Table 1: Calculated values for AOT surfactant…….…….....9

Table 2: Calculated mass fraction for reverse micelle prepared with *w* = 10……....27

Table 3: Experimental concentrations selected for the aqueous salt precursors……...…30

Table 4: Commercial gold colloids in aqueous media…….……..32

Table B-1. Group molar attraction constant……..54

Table C-1. Volumetric fraction (ϕ_{vol}) of gold colloid standards in aqueous media and in water/AOT/isooctane solution…….56

Table D-1. Theoretical yield obtained from experimental concentrations of the aqueous salt precursors……..…57

Table D-2. Volumetric fraction (ϕ_{vol}) of gold nanoparticles synthesized in reverse micelles with *w* = 10……58

1. INTRODUCTION AND BACKGROUND

1.1 Introduction

In a talk given in 1959, Richard Feynman suggested that devices and materials could someday be fabricated to atomic specifications [1]. The materialization of Feynman's vision is the field now called Nanotechnology, a discipline that encompasses work at the nanometer scale (1nm = 10^{-9} m = 10 Å), providing the real possibility for controlling the structure of matter at the molecular level. As such, nanotechnology is widely viewed as the most significant technological frontier currently being explored. Figure 1 shows a relation between the size of a natural biological structure and one constructed from the application of human ingenuity.

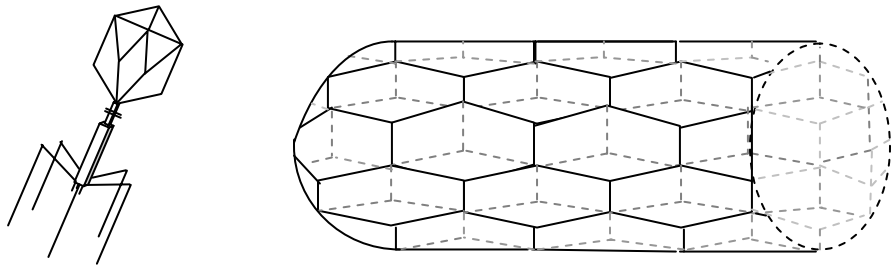

A) T-2 Phage virus (100 nm) B) Carbon nano-tube (200-500 nm)

Figure 1: Comparison of sizes of two nano-structures: A) biological configuration of a virus and, B) carbon nano-wire arrangement.

Metal particles are a particularly interesting nanoscale system because of the ease with which they can be synthesized and modified chemically [2]. Furthermore, they often offer an advantage over other systems because their optical properties (as described through the dielectric constant) differ from those of the bulk metal [3, 4]. This effect is in part due to the fact that metal nanoparticles exhibit strong plasmon resonance absorption

bands in the visible spectrum and therefore produce deep colors reminiscent of molecular dyes. These bands can often be rationalized in terms of classical free-electron theory and electrostatic models for particle polarization [5].

The foremost metal nanoparticles under study are silver (Ag), copper (Cu) and gold (Au). Gold nanoparticles in particular have been extensively investigated due to their unique physical and chemical properties and wide potential applications [6] as in bioassays [7], where colloidal gold nanoparticles are used as protein tags to amplify the signal from a surface plasmon resonance biosensor. As another example, gold nanoparticles allow the induction of dehybridization of a DNA sequence (Figure 2) using a radio-frequency magnetic field to heat a gold nanoparticle attached to a DNA chain [8].

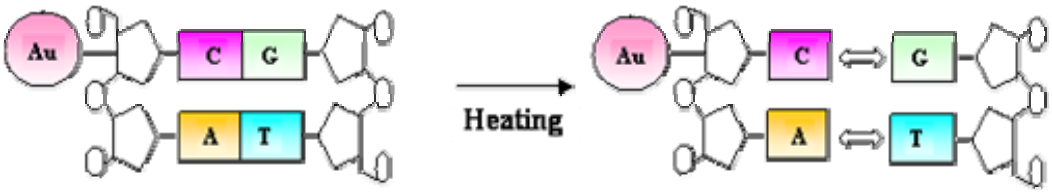

Figure 2: Use of gold nanoparticle as tag to promote DNA dehybridization process.

We investigated the use of reverse micelles prepared in the system water, sodium bis-2(ethylhexyl) sulfoccinate (AOT), and isooctane as templating system for the synthesis of gold nanoparticles, determining their shape and size characteristics through spectroscopy and microscopy techniques.

1.2 Background

A wide range of techniques for the synthesis of gold nanoparticles have been developed in recent years with the objective of controlling the size and shape of the resulting nanoparticles. Among them, the use of reverse micelles as nanoreactors, which allow better control over the final characteristics of the nanoparticles, emerges as a particularly promising approach.

1.2.1. Reverse Micelles

Reverse micelles consist of aqueous droplets that are separated from the bulk organic phase by a surfactant layer, as illustrated in Figure 3. This is an isotropic and thermodynamically stable single-phase system that consists of three components: water, organic solvent, and an amphiphiillic molecule, the surfactant [9].

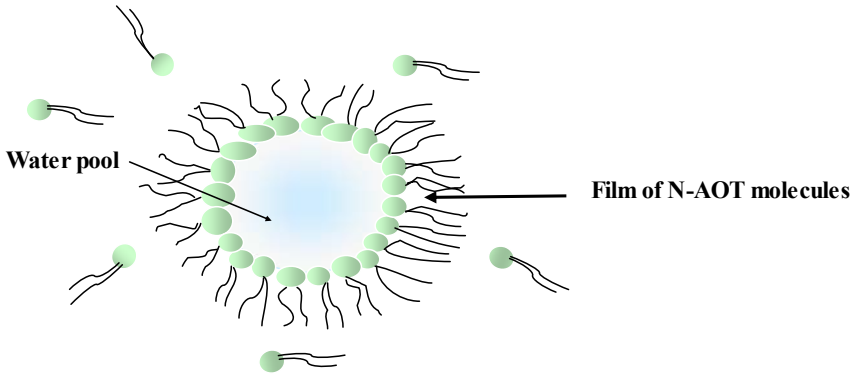

Figure 3: Conceptual illustration of a reverse micelle system.

Surfactants are molecules that possess a hydrophilic head group and a hydrophobic tail group. They can be anionic, cationic, or nonionic in nature. All of these factors contribute to the behavior of surfactants in solution. Surfactants have a tendency to self-

assemble into structures that are dependent upon their character and environment. Structures such as spheres, cylinders, bi-layers, lamellar sheets, or inter-contiguous networks are possible depending on the hydrophobic and hydrophilic interactions between surfactant molecules and their environment. Some of these structures are illustrated in Figure 4.

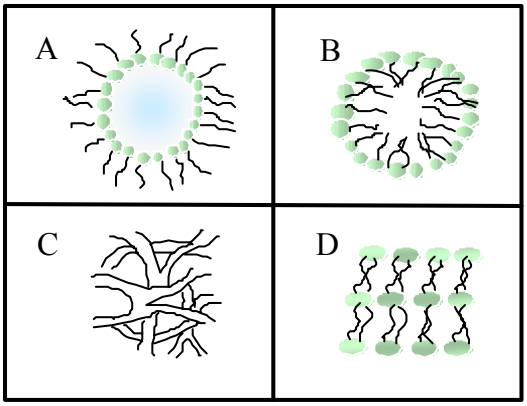

Figure 4: Illustration of micellar morphologies: reverse micelle (A), normal micelle (B), interconnected cylinders (C), planar lamellar phase (D).

The balance of forces between the polar head groups of the surfactant molecules and the orientation of their tails allows the self assembly of the surfactant into well defined structures such as reverse micelles. The hydrophilic head groups are in contact with the water interface and experience mutual steric repulsion. This force is opposite to the interfacial attraction between the hydrophobic tails and the organic solvent; this equilibrium tends to determine the effective area per surfactant molecule (a) in the aqueous-organic interfaces, with a typical surface tension (γ) of 50×10^{-3} N/m [10]. This balance of forces is illustrated in Figure 5.

The free energy (μ_N°) per surfactant molecule in a specific aggregate structure can be written as [11]:

$$\mu_N^{\circ} = \Phi_A + \Phi_R + g \ , \tag{1.1}$$

in which, Φ_A represents the attraction energy, Φ_R the repulsion energy, and g is the bulk free energy contribution.

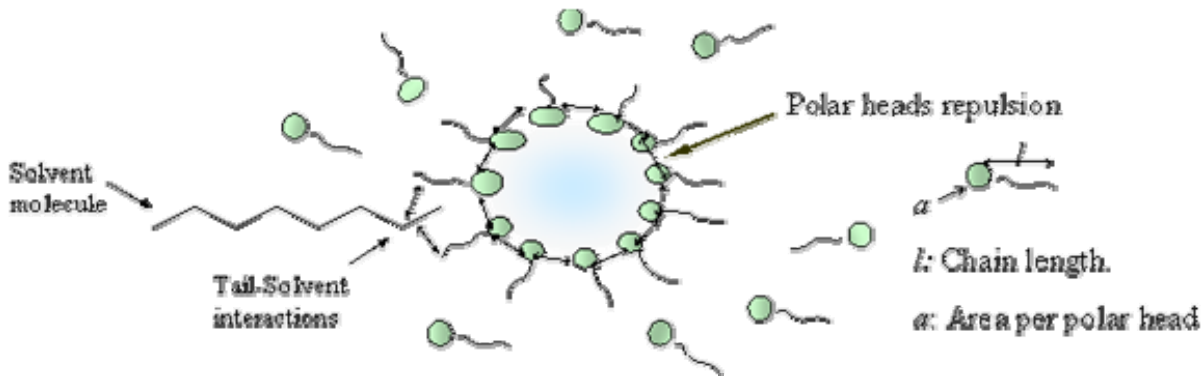

Figure 5: Principal forces acting on a reverse micelle.

The attractive energy is given by the surface tension (γ) of the aqueous-organic interface and the area of the surfactant molecules (a). To determine the repulsion energy in terms of distribution of charge per surfactant, a capacitor model [10] which relates the surface charge density (ρ^*) to the separation distance (δ) between the capacitor planes may be used; the separation distance is related to the double layer thickness from electrostatic theory [12]. The surface charge density (ρ^*) can be expressed as:

$$\rho^* = \frac{q}{a}, \tag{1.2}$$

where q is the charge per surfactant molecule. The electric field induced in the capacitor model is proportional to the charge density and inversely proportional to the dielectric constant of the surfactant molecules:

$$E = \frac{\rho^*}{\varepsilon} = \frac{q}{\varepsilon\, a}. \tag{1.3}$$

We can also express the repulsion energy in terms of Coulomb's law:

$$\Phi_R = F\ \delta, \tag{1.4}$$

in which F is the force of repulsion. The electric field (E) is defined by:

$$E = \frac{F}{q}\ . \tag{1.5}$$

Therefore

$$\Phi_R = Eq\delta = \frac{q^2\delta}{\varepsilon a}. \tag{1.6}$$

Substituting equation (1.6) in equation (1.1) it is possible to calculate the free energy per surfactant molecule (μ_N°):

$$\mu_N^\circ = \gamma a + \frac{q^2\delta}{\varepsilon a} + g\ . \tag{1.7}$$

A stable self assembled structure tends to achieve a minimum free energy per unit area [11]:

$$\frac{d\mu_N^\circ}{da} = 0 = \gamma - \frac{q^2\delta}{\varepsilon a^2}, \tag{1.8}$$

from this last equation, an expression for the effective area per surfactant molecule may be obtained:

$$a = \sqrt{\frac{q^2 \delta}{\varepsilon \gamma}} \,. \tag{1.9}$$

Another important parameter necessary to understand how the surfactant forms a specific structure spontaneously is the surfactant parameter or "packing parameter", defined as (*v/al*), where *v* is the volume of the surfactant molecule and *l* is the characteristic length of the hydrophobic section [9, 11, 13]. The *v* parameter is viewed as the volume occupied by an alkyl chain of n_c carbon atoms, and is deduced from the empirical volume additivity rule of Traube [14]. The length of the hydrophobic section (*l*) is defined as the maximum possible extension of a hydrocarbon chain, and also is a function of the number of carbon atoms. The following expressions are useful to calculate the values of *v* and *l* [13, 15, 16]:

$$v = 27.4 + 26.9\, n_c \ (\text{Å}^3 / \text{chain}) \,, \tag{1.10}$$

$$l = 1.5 + 1.265\, n_c (\text{Å}) \,. \tag{1.11}$$

Small values of the packing parameter imply highly curved aggregates such as in spherical micelles [$(v/al) < 0.33$] and infinite cylinders [$0.33 < (v/al) < 0.5$]. When (v/al) is close to unity, planar bilayers usually form; inverted cylinders and micelles are obtained for $(v/al) > 1$ [9].

Sodium bis(2-ethylhexyl) sulfosuccinate (AOT) is one of the most commonly employed surfactants in forming microemulsions [17-19]. Its molecular shape allows high water solubilization with the formation of a well defined aqueous organic interface. Figure 6 is an illustration of the AOT molecule.

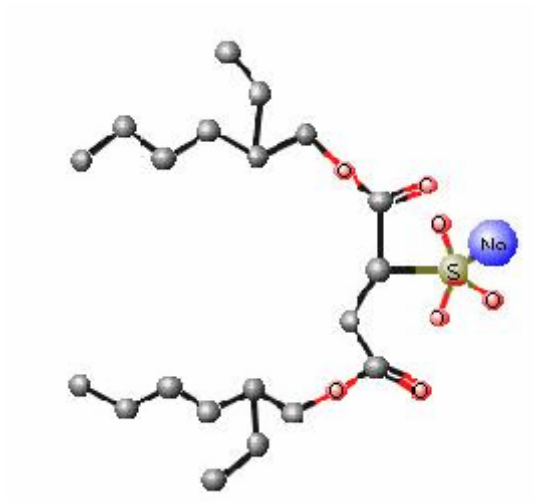

Figure 6: Structure of Aerosol OT. Carbon molecules are represented by grey spheres, oxygen molecules by red spheres, and sulphur and sodium molecules by yellow and blue spheres respectively.

In micellar systems, AOT has a charge per molecule (q) equivalent to 3.668×10^{-18} C [20], a double layer thickness (δ) of ~5 Å [10, 11], and a dielectric constant (ε) in isooctane equal to 3.530×10^{-10} C^2/Jm [10], or in dimensionless form $\varepsilon/(4\pi\varepsilon_0)$ is equal to 3.184 ($\varepsilon_0 = 8.825\times10^{-12} C^2/Jm$); this value matches very well with the reported value for AOT micelles formed in n-heptane (ε =3.4) [19].

Substituting the values of q and ε for AOT molecules in isooctane into equation (1.9) it is possible to calculate the area per polar head group in the aqueous-organic interface. Furthermore, applying equations (1.10) and (1.11) we obtain the molecular volume and the chain length for the AOT molecule, and in this way, the surfactant packing parameter, shown in Table 1.

Table 1: Calculated values for AOT surfactant

AOT parameter	Calculated value
A	61.72 $Å^2$
V	592.8 $Å^3$
L	9.09 Å
(*v/la)*	1.056

A surfactant molecule lowers the interfacial tension between water and the organic solvent, resulting in the formation of a transparent solution. Using reverse micelles to synthesize nanostructures takes advantage of the small size of the micellar water pools, which essentially act as nanoreactors [21]. These nanoreactors collide continuously due to thermal Brownian motion. The system chosen for this investigation has an upper collision rate (*Z*) of about 3.91×10^3 s^{-1}, as shown in Appendix A, hence a fraction of droplets exist in the form of short-lived dimers which exchange their water content [12]. After a short time these dimers separate to form two droplets (as illustrated in Figure 7). As a result of this coalescence and separation mechanism, molecules solubilized in the water pools are redistributed over the micellar population [22].

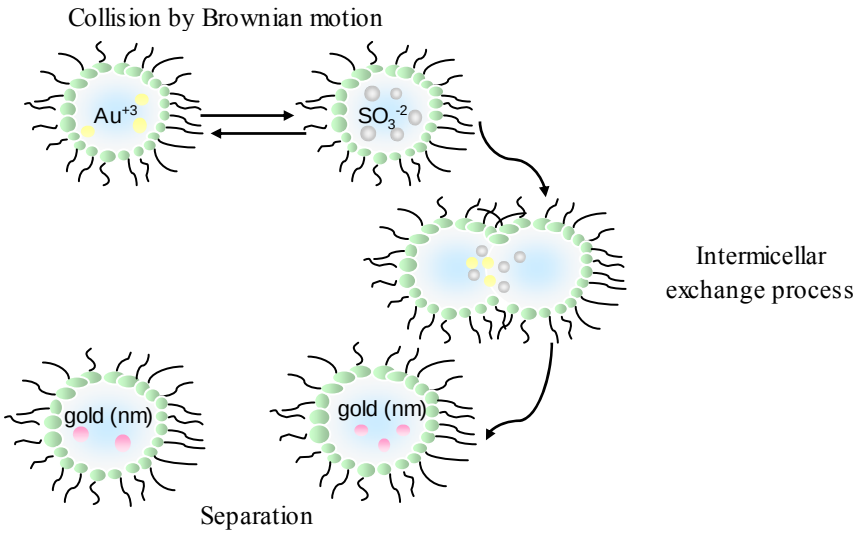

Figure 7: Illustration of the micellar exchange process.

The capacity to exchange materials between water droplets depends on the interfacial flexibility, which is related to the bending elastic modulus and the rate constant of the exchange mechanism. The bending modulus or bending elastic/rigidity constant (κ) [22] is equal to twice the amount of elastic energy (E_{el}) required to bend a unit of area by unit of curvature.

$$\kappa = 2E_{el}R_h . \tag{1.12}$$

The elastic force (F_{el}) and elastic energy (E_{el}) can be defined from Hook's law as

$$F_{el} = kR_h , \tag{1.13}$$

$$E_{el} = \frac{1}{2}kR_h^2 , \tag{1.14}$$

where k is the elastic constant, and R_h is the hydrodynamic radius.

The relaxation time for surface deformation (τ) is obtained from a force balance between the elastic force (F_{el}) and the contribution of a friction factor (f) on the deformation of reverse micelle surface with time:

$$\frac{\kappa}{R_h} = f\frac{\partial R_h}{\partial t} \ , \tag{1.15}$$

integrating equation (1.15) we obtain an expression for τ [23]:

$$\tau = \frac{fR_h^2}{\kappa} \ , \tag{1.16}$$

using Stokes law for f ($f = 6\pi R_h \eta$), we obtain:

$$\tau = \frac{6\pi\eta R_h^3}{\kappa} \ . \tag{1.17}$$

The bending modulus κ also depends on the interaction between the molecules of the organic solvent and the surfactant tails. A large value of the bending modulus makes the interface more rigid and hinders coalescence and material exchange between the reverse micelles [24].

When the intrinsic chemical reaction kinetics is too fast, the overall reaction rate is controlled by the material exchange rate (K_{ex}) [25], a second order constant with units $[sM]^{-1}$. K_{ex} can be related to the collision frequency of droplets, assuming a diffusion controlled rate constant (K_{DC}) [21, 24]. This constant is deduced from the Stokes-Einstein relation

$$K_{DC} = \frac{8RT}{3000\eta} \ , \tag{1.18}$$

where R is the gas constant, T the absolute temperature, and η the solvent viscosity; a conversion factor is used for consistent SI units.

The characteristic time (t) between collisions is defined as the reciprocal of the collision rate (Z) [22]:

$$t = \frac{1}{Z} \tag{1.19}$$

For water/AOT/isooctane reverse micelles prepared with w = 10, we obtain a characteristic time between collisions of 25.5 μs (as shown in Appendix A).

The free energy (μ_N°) of a reverse micelle structure formed by a determined micellar aggregation number of surfactant (N) in equilibrium with a free mole fraction (x) of surfactant can be written as [16]:

$$\mu_N^\circ + \frac{k_B T}{N} * ln\left(\frac{x_N}{N}\right) = \mu_1^\circ + k_B T * ln\left(x_1\right), \tag{1.20}$$

in which $k_B T$ is the thermal energy (where k_B is Boltzmann's constant: 1.3806×10^{-23} J/K), x_N, and x_1 are the mole fraction of the surfactant in the aggregate structure and in the bulk solvent respectively [10]. Figure 8 illustrates a scheme of this association.

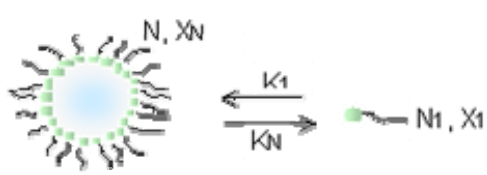

Figure 8: Representation of micellar association kinetics in a reverse micelle.

Then

$$ln\left(\frac{x_N}{N}\right) = \frac{N}{K_B T}\left\{\left(\mu_1^\circ - \mu_N^\circ\right) + K_B T\ lnx_1\right\} \tag{1.21}$$

$$x_N = N\exp\left\{\frac{N\left(\mu_1^\circ - \mu_N^\circ\right)}{K_B T} + N\ lnx_1\right\}, \tag{1.22}$$

$$x_N = Nx_1^N \exp\left\{\frac{N\left(\mu_1^\circ - \mu_N^\circ\right)}{K_B T}\right\}, \tag{1.23}$$

from equation (1.23) it is possible to establish a new parameter, the dimensionless total surfactant molecule concentration, which is expressed as [9, 16]

$$C = \sum_{N=1}^{\infty} x_N\ , \tag{1.24}$$

at low concentrations, most of the surfactant molecules in solution do not form aggregates, and behave as isolated monomers. The mean concentration at which micellization begins to occur is commonly referred to as the Critical Micelle Concentration (*CMC*) [9], and is related to the minimum concentration of the surfactant that is needed so that the surfactant molecules begin to associate and form clusters or aggregates, according to thermodynamic equilibrium considerations.

The minimum concentration or mole fraction of surfactant molecules at which aggregates can form is defined as x_{1crit} and is given by [10, 24]:

$$x_{1crit} = CMC = \exp\left[\frac{-\left(\mu_1^\circ - \mu_N^\circ\right)}{K_B T}\right], \tag{1.25}$$

the *CMC* can be determined by techniques such as conductance measurements [25], and time resolved luminescence [23, 26]. An experimental measurement of the *CMC* for AOT in isooctane is 0.00810 M [12].

The size of the reverse micelle greatly influences the size of the resulting nanoparticles. An interesting parameter to be determined in order to characterize a reverse micelle as regards to its size is the radius of its water droplet (R_w). This parameter is dependent on the water to surfactant molar ratio (w) used to prepare the micellar solution [20].

$$w = \frac{[H_2O]}{[AOT]}. \tag{1.26}$$

A basic relationship between R_w and w was proposed by Pileni [16, 27], based on geometrical considerations assuming the water pool as a spherical structure with a total volume (V) formed by free water molecules with a molecular volume (v_w) of 30 Å^3 at 25°C [23]. Hence,

$$V = v_w w N, \tag{1.27}$$

where N was previously related with the micellar aggregation number. The total interfacial area (S) of a reverse micelle structure is given by the product of the area per polar head (a) and the micellar aggregation number (N)

$$S = aN, \tag{1.28}$$

using a value of area per polar head of AOT of about 60 Å^2 [11, 28], V and S can be related as:

$$\frac{V}{S} = \frac{1}{2} w\,(\text{Å}), \tag{1.29}$$

moreover, from geometrical considerations the relation between V and S is given by:

$$\frac{V}{S} = \frac{1}{3} R_w\ (\text{Å}), \tag{1.30}$$

comparing equations (1.29) and (1.30) one obtains an expression for R_w as a function of w.

$$R_w = 1.5 w\,(\text{Å}). \tag{1.31}$$

It is important to remark that this relation does not take into account collisions between micelles, or their diffusion coefficient (D).

The hydrodynamic radius (R_h) of the micelle, which includes the contribution of the surfactant layer thickness may be determined experimentally through different techniques such as Dynamic Light Scattering (DLS) [22, 29-31], time resolved luminescence [23, 26], Small Angle Neutron Scattering (SANS) [13, 32, 33], and Small Angle X-ray scattering [15].

The ternary phase diagram for the system water/AOT/isooctane at a temperature of 298 K [9, 34] is presented in Figure 9. There we illustrate some of the different micellar phases that can be obtained by properly selecting the value of the water to surfactant molar ratio (w) used in the preparation of the micellar solutions. The equilibrium of these micellar phases depended on thermodynamic considerations, and could be affected by changes in temperature, and electrolyte concentrations.

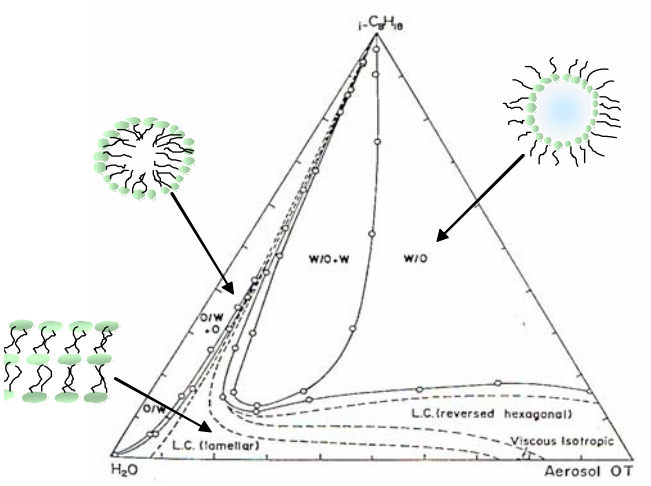

Figure 9: Phase Diagram for AOT/Isooctane/Water ternary system at 298 K. Oil in water (O/W: micelles), water in oil (W/O: reverse micelles), and lamellar sheets. Adapted from [9].

Another important factor in the study of reverse micelles for the synthesis of nanoparticles is the stability of the system. Depending on the preparation conditions, the particles could have a tendency to agglomerate slowly and flocculate [35]. Some alcohols and poly-ethylene ethers (C_iE_j) have been used as cosurfactants in order to enhance the stability of the reverse micelles [17, 25]. Depending on their solubilization site, they can affect the interface rigidity and in this way, the rate of exchange of material between micelles.

1.2.2. Mie Theory

The optical properties of gold nanoparticles have been intensively investigated during recent years, particularly with respect to their size dependence. Of particular interest is the light extinction process in the UV-visible range, which occurs when an electromagnetic wave passes through a metal particle exciting its electronic or vibrational states. This phenomenon induces dipole moments that oscillate at the respective

frequency of the incident wave, and therefore disperse secondary radiation in all directions [36]. This collective oscillation of the free conduction electrons is called plasmon resonance [4], and is illustrated in Figure 10.

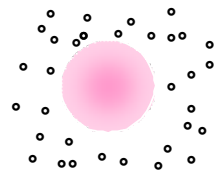

a) Collective oscillation of the free conduction electrons around a gold atom

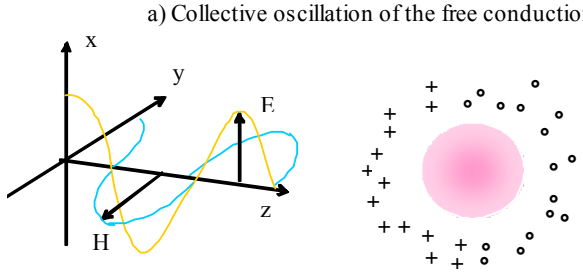

b) Effect of plasmon resonance on a gold nanoparticle interacting with an electromagnetic field

Figure 10: Plasmon resonance phenomena.

The extinction spectra of a fairly dilute dispersion of colloidal metal particles can be explained using Mie's Theory [37], a mathematical-physical description of the scattering of electromagnetic radiation by spherical particles. This theory was developed by Gustav Mie in 1908, and assumes non-interacting spherical isotropic particles in a non-absorbing medium. A solution for single scattering in the far field limit is thus obtained.

Considering a spherical particle exposed to an electromagnetic wave which crosses the surface with a net rate of absorption (W_a) [5].

$$W_a = -\int_A S.\hat{e}_r dA\,, \tag{1.32}$$

in which S is the pointing vector that specifies electromagnetic energy flux, $\hat{e}_r$ is a unit normal vector in the radial direction, and dA the differential surface area. The net rate of light extinction (W_e) due to the particle can be deduced from an energy balance in terms of the rate of incident light (W_i) and the scattered radiation (W_s). Figure 11 gives a representation of these energy transfer mechanisms.

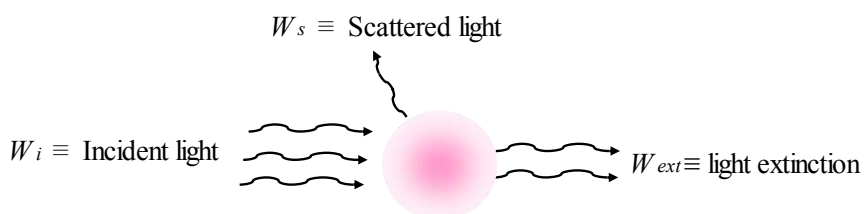

Figure 11: Energy transfer from the absorption of light by a spherical particle.

Then we have

$$W_a = W_i - W_s + W_{ext}, \tag{1.33}$$

For a non absorbing medium, W_i tends to vanish [37], resulting in:

$$W_{ext} = W_a + W_s. \tag{1.34}$$

A common way to express the net rate of electromagnetic wave extinction (W_{ext}) is in terms of the extinction cross section (C_{ext}):

$$C_{ext} = \frac{W_{ext}}{I_i}, \tag{1.35}$$

where I_i is the incident irradiance. The extinction coefficient (C_{ext}) is a measure of the reduction in the intensity of transmitted light for a specific medium and can be expressed as [5, 37, 38]:

$$C_{ext} = \frac{2}{x^2}\sum_{n=1}^{\infty}(2n+1)[\mathrm{Re}(a_n + b_n)], \tag{1.36}$$

in which

$$x = kR = \frac{2\pi n_o R}{\omega}, \tag{1.37}$$

in these equations k is the wave number vector, R is the radius of the particle, n_o is the refractive index of the host medium, ω is the wavelength of the incident light *in vacuo,* and a_n and b_n are the scattering coefficients which are expressed in terms of Riccati-Bessel functions.

In order to obtain specific relations for the scattering coefficients, first we must consider the configuration of an incident electromagnetic field which has two components, the electric field $\boldsymbol{E}$, and the magnetic field $\boldsymbol{H}$ is perpendicular; Helmholtz's equations (1.38) describe this system [5, 37]

$$\nabla^2 \boldsymbol{E} + k^2 \boldsymbol{E} = 0 \text{ and } \nabla^2 \boldsymbol{H} + k^2 \boldsymbol{H} = 0, \tag{1.38}$$

The solutions of Helmholtz's equations are linear combinations ($\boldsymbol{M}$, $\boldsymbol{N}$) defined in terms of a scalar function (ψ):

$$\boldsymbol{M} = \nabla \times \boldsymbol{r}\psi \text{ and } \boldsymbol{N} = \frac{1}{k}\nabla \times \boldsymbol{M}, \tag{1.39}$$

to resolve $\boldsymbol{M}$ and $\boldsymbol{N}$ in terms of the spherical coordinates (r,θ,φ), it is necessary to apply the method of separation of variables on the scalar function (ψ):

$$\psi = R(r)\Theta(\theta)\Phi(\phi), \tag{1.40}$$

using spherical Bessel functions and a Legendre polynomial, the separation functions *R(r)*, *Θ(θ)*, and *Φ(ϕ)* are obtained

$$\begin{aligned} &r : R(r) = \left\{ j_n(r),\ or\ y_n(r),\ or\ h_n^{(1)},\ or\ h_n^{(2)} \right\} \equiv z_n(r), \\ &\theta : \Theta(\theta) = P_n^m(\cos\theta), \\ &\phi : \Phi(\phi) = \sin(m\phi). \end{aligned} \tag{1.41}$$

The solution for ψ will have odd and even components

$$\begin{aligned} \psi_e &= \cos(m\phi) P_n^m(\cos\theta) z_n(r), \\ \psi_o &= \sin(m\phi) P_n^m(\cos\theta) z_n(r). \end{aligned} \tag{1.42}$$

The boundary conditions around a spherical particle interacting with an electromagnetic field are given by

$$\begin{aligned} \hat{\boldsymbol{n}} \times \left(\boldsymbol{H}_2 - \boldsymbol{H}_1 \right) = 0 \\ \hat{\boldsymbol{n}} \times \left(\boldsymbol{E}_2 - \boldsymbol{E}_1 \right) = 0 \end{aligned} \tag{1.43}$$

in which, $\hat{\boldsymbol{n}}$ is the unit vector, and the subscripts *1* and *2* are related to the interior and exterior of the spherical particle respectively. Using the solutions found for the electromagnetic field (***E, H***), equation (1.43) can be expressed as:

$$\begin{aligned} &j_n(mx) c_n + h_n^{(1)}(x) b_n = j_n(x), \\ &\mu \left[mx j_n(mx) \right] + \mu_1 \left[x h_n^{(1)}(x) \right] b_n = \mu_1 \left[x j_n(x) \right], \\ &\mu m j_n(mx) d_n + \mu_1 h_n^{(1)}(x) a_n = \mu_1 j_n(x), \\ &\left[mx j_n(mx) \right] d_n + m \left[x h_n^{(1)}(x) \right] a_n = m \left[x j_n(x) \right], \end{aligned} \tag{1.44}$$

where x was defined in equation (1.37), and m is the relative refractive index. Solving the system of equations described in equation (1.44) it is possible to find expressions for the scattering coefficients a_n and b_n in terms of the Ricatti-Bessel functions $\psi_n(x)$ and $\xi_n(x)$:

$$a_n = \frac{m\psi_n(mx)\psi_n^{'}(x) - \psi_n(y)\psi_n^{'}(mx)}{m\psi_n(mx)\zeta_n^{'}(x) - \zeta_n(x)\psi_n^{'}(mx)},$$

$$b_n = \frac{\psi_n(mx)\psi_n^{'}(x) - m\psi_n(y)\psi_n^{'}(mx)}{\psi_n(mx)\zeta_n^{'}(x) - m\zeta_n(x)\psi_n^{'}(mx)}. \tag{1.45}$$

For isolated dilute gold nanoparticles with radius (R) smaller than the wavelength of visible light (λ) an optical response occurs when an electromagnetic field is applied [5, 39], which is manifested through the polarization of charges (σ) of the free conduction electrons. The movement of these charges tends to have a resonance due to equilibrium considerations, described by [5]

$$\sigma = 4\pi\varepsilon_o R^3 \frac{\varepsilon - \varepsilon_m}{\varepsilon + 2\varepsilon_m}, \tag{1.46}$$

where ε_m is the dielectric constant of the surrounding medium, and ε is the dielectric constant of the gold particle. The value of ε for metal particles is obtained by taking into account the contribution of its real and imaginary parts [40]

$$\varepsilon = \varepsilon_1(\omega) + i\varepsilon_2(\omega) = (n + i\kappa)^2, \tag{1.47}$$

in which n is the index of refraction, and κ is related to light absorption. For free electron metals it has been found that ε_2 (ω) is a constant in the UV-Visible range and hence maximum absorption occurs when $\varepsilon_1(\omega) = -2\ \varepsilon_m$, due to the dipole-plasmon resonance effect [37].

One relevant modification to Mie theory considers the scattering of light from spheres coated with a homogeneous layer of uniform thickness of an absorbing medium with dielectric properties different from that of the core and surrounding medium [5, 37]. The

electromagnetic radiation scattered from this core-shell geometry can be described in the same form as that scattered from a homogeneous sphere by considering the influence of the radial variation of the scattering coefficients a_n and b_n on the extinction cross section [37]. The scattering coefficients are now given by

$$a_n = \frac{\psi_n(y)\left[\psi_n^{'}(m_2 y) - A_n \chi_n^{'}(m_2 y)\right] - m_2 \psi_n^{'}(y)\left[\psi_n(m_2 y) - A_n \chi_n(m_2 y)\right]}{\xi_n(y)\left[\psi_n^{'}(m_2 y) - A_n \chi_n^{'}(m_2 y)\right] - m_2 \xi_n^{'}(y)\left[\psi_n(m_2 y) - A_n \chi_n(m_2 y)\right]},$$

$$b_n = \frac{m_2 \psi_n(y)\left[\psi_n^{'}(m_2 y) - B_n \chi_n^{'}(m_2 y)\right] - \psi_n^{'}(y)\left[\psi_n(m_2 y) - B_n \chi_n(m_2 y)\right]}{m_2 \xi_n(y)\left[\psi_n^{'}(m_2 y) - B_n \chi_n^{'}(m_2 y)\right] - \xi_n^{'}(y)\left[\psi_n(m_2 y) - B_n \chi_n(m_2 y)\right]}, \tag{1.48}$$

$$y = kR_p \tag{1.49}$$

where $\psi_n(y)$ and $\xi_n(y)$ are Ricatti-Bessel expressions, m_1 and m_2 are the refractive indices of the core and coating relative to the adsorbing medium, and R_p is the radius of the coated particle.

The shell material can be a metal, or any other kind of material such as a surfactant or polymer [41, 42]. A representative scheme of this core shell structure is shown in Figure 12, in which the distribution of the dielectric constant of the core (ε_c), shell (ε_{sh}), and medium (ε_m) are illustrated. An example of the advantages of using this core shell model was presented by Baer and co-workers [43], who have investigated the use of metallic nanoshells to enhance absorption of metallic dots in order to develop photonic probes for imaging purposes.

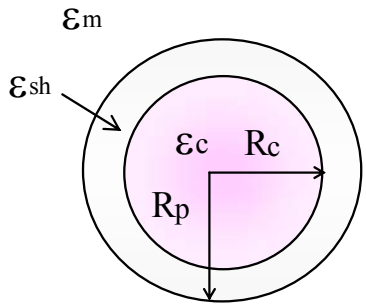

Figure 12: Core shell spherical particle.

2. PREVIOUS WORK

Spectrophotometer techniques have been previously applied to study the synthesis, growth, and initial kinetics of producing metallic nanoparticles from Au^{+3} and Ag^{+} [44, 45] in aqueous medium. These previous contributions serve as basis for the work presented here, wherein we intend to study the formation of gold nanoparticles in a radically different medium: reverse micelles formed in the system water/AOT/isooctane.

2.1 Synthesis and growth of Gold nanoparticles in Aqueous Media

Murillo and co-workers [44] have studied the formation of gold nanoparticles in aqueous solution. In their system, the reduction, nucleation, and growth process took less than 1 s and required a particularly fast technique to follow the optical changes. For this reason, a stopped flow reactor (SFR) was used. In their work, the optical properties of the metallic particles and the gold plasmon resonance were followed using Mie's theory, as developed for a single spherical particle.

A complete reduction of Au^{+3} was obtained in about 20 ms. Plasmon resonance due to metallic behavior was associated with the peak at 525 nm [45]. From this work, a time dependent spectrum for reduction and growth of gold nanoparticles was obtained, in which was observed a regime of regular particle growth after 0.4 s.

2.2 Synthesis of Gold nanoparticles using reverse micelles

As illustrated in Figure 13, synthesis of gold nanoparticles using reverse micelles involves the preparation of two identical water-in-oil microemulsions with a specific water to surfactant molar ratio (*w*). The reactants used are a metallic salt (A) and a reduction agent (B) that are dissolved in the aqueous phases of these two microemulsions [46, 47]. Upon mixing, collisions and droplet coalescence bring the reactants A and B into contact to form the gold nanoparticle product inside the reverse micelles.

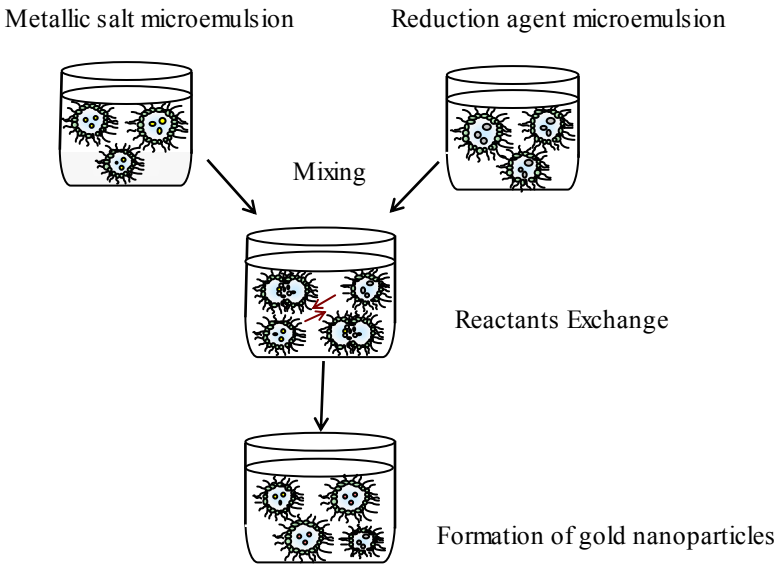

Figure 13: Schematic representation of synthesis of gold nanoparticles in reverse micelles.

Wilcoxon and co-workers [48] have studied the synthesis of gold nanoparticles formed in aqueous media and in reverse micelles, using chemical and photolytic reduction methods. The chemical reduction method was achieved using reduction agents such as hydrazine, sodium borohydride, and metallic sodium (the latter was used in the synthesis of gold colloids in micelles) with different auric salts, among them $NaAuCl_4$ and $KAuBr_4$. They observed, from extinction measurements, a blue-shift with decreasing particle size, an observation in agreement with Mie theory [4]. Measurements of the hydrodynamic diameter of gold nanoparticles synthesized in aqueous media and in reverse micelle solutions were made using Dynamic Light Scattering (DLS). From these measurements, they observed larger sizes for nanoparticles in reverse micelles. This was attributed to the metallic nature of gold colloids, which contribute to increasing the intensity of scattered light from micellar media.

Chiang and co-workers [46] have synthesized gold nanoparticles from mixed reverse micelles formed with anionic surfactant (AOT) and nonionic cosurfactant (Tetraethylene glycol dodecyl ether: $C_{12}E_4$) in isooctane. For this purpose, they used tetrachloroauric acid ($HAuCl_4$) with hydrazine as reducing agent. They obtained a particle size distribution of 8.2 to 21.5 nm, with a mean diameter of 14.3 ± 2.4 nm for a water surfactant molar ratio (w) of 8.0 with three times excess of reducing agent.

The use of a cosurfactant allows better control of the final nanoparticle size. When the concentration of $C_{12}E_4$ was increased from 0.05 to 0.2 M, the particle diameter decreased from 43.7 to 14.3 nm. Stabilization of the nanoparticles was achieved by

enhancing the reverse micelle structure preventing further growth and precipitation. This was attributed to the solubilization site of $C_{12}E_4$ in the reverse micelles [17], in which it is assumed that the head groups are immersed in the water pool.

Fengxin Chen and co-workers [49] have studied the preparation of colloidal gold nanoparticles in CTAB (Cetyl Trimethyl Ammonium Bromide) stabilized in n-pentanol/hexane/water to form a reverse microemulsion. They were able to prepare monodisperse and stable gold colloids with an average particle diameter of 7 nm.

Lin and co-workers [47] have determined a stronger van der Waals interaction between n-pentanol and CTAB, which ensures the formation of a more compact and stable interfacial film in the reverse micelle system used to synthesize gold nanoparticles from $HAuCl_4 3H_2O$ and $NaBH_4$. The microemulsion prepared with $NaBH_4$ was added dropwise to the microemulsion containing the metal salt. The solution quickly changed from a crystalline red, to a colorless solution, then to crystalline yellow, and finally to deep dark red upon addition of $NaBH_4$. UV-VIS spectra obtained in this study showed a typical surface plasmon absorption band with λ_{max} at 524 nm.

3. MATERIALS AND METHODS

3.1 Reactants

The metal salt was auric potassium tetrachloride ($KAuCl_4$), and the reducing agent was potassium sulfite (K_2SO_3) purchased from Sigma Aldrich. Gold colloids with

diameters of 5 to 100 nm were acquired from Ted Pella Inc. Sodium bis-(2-ethylhexyl) sulfosuccinate (AOT) 99% was purchased from Sigma, and 2,2,4-trimethylpentane (isooctane) was acquired from Fisher. Deionized and degasified water was used in all preparations.

3.2 Determination of reverse micelle size

We prepared reverse micelles using the system water/AOT/isooctane, with specific water to surfactant molar ratio (w) of 10; we choose this value as it allow us to work well within the water-in-oil emulsion region of the water-AOT-isooctane phase diagram. The mass fractions (x) used for reverse micelles preparations are shown in Table 2; a representative phase diagram obtained with these mass fractions is illustrated in Figure 14, in which we observe that reverse micelles prepared with $w = 10$ have a well defined structure.

Table 2: Calculated mass fraction for reverse micelle prepared with $w = 10$ relation.

Composition	***x* (%)**
Aqueous phase	0.103
AOT	0.252
Isooctane	0.644

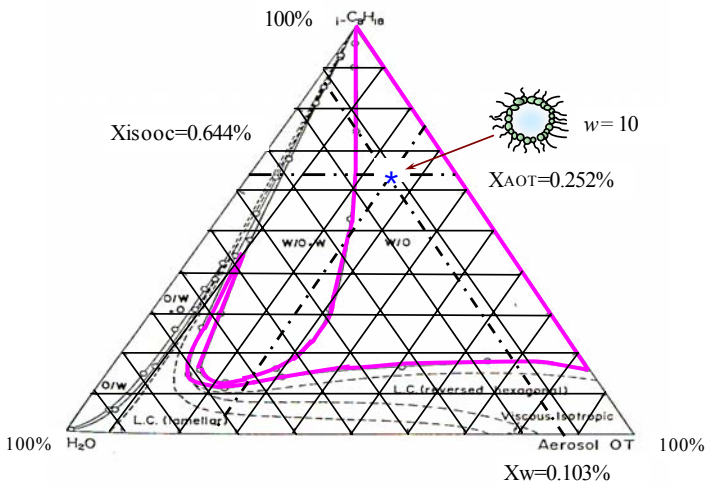

Figure 14: Phase diagram for reverse micelle w=10: Aqueous/AOT/Isooctane.

We assumed that the water pool is formed by free water molecules, neglecting the presence of water molecules hydrating the AOT film, or water molecules dispersed at the micellar periphery [27, 28], as shown in Figure 15.

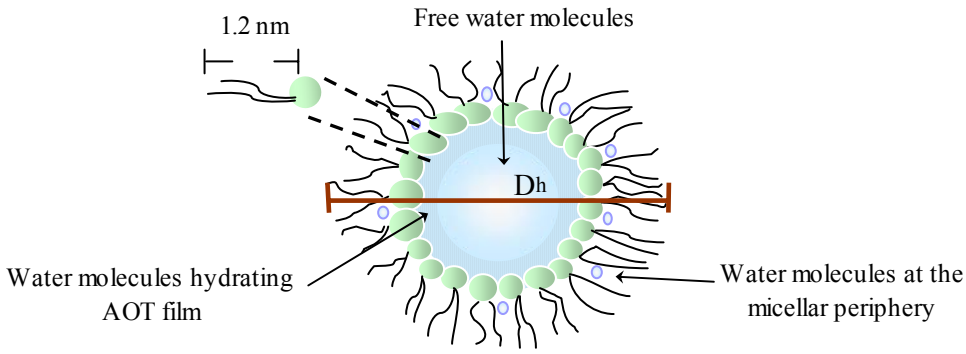

Figure15: Conceptual illustration of reverse micelle structure.

The diameter of the water pool is believed to control the final nanoparticle size [13, 15]. This diameter was estimated by measuring the reverse micelle hydrodynamic diameter (D_h) and subtracting the thickness of the surfactant layer, which for AOT is

about 1.2 nm [22]. We used Dynamic Light Scattering (DLS) to measure the hydrodynamic diameter as a function of the water to surfactant molar ratio (w) [29-31], using a 90 Plus Particle Size Analyzer from Brookhaven Instruments Corp. These results are shown in Figure 16, and a linear regression of D_h vs w yields equation (3.1). From this relation, we estimate that the hydrodynamic diameter for AOT/water/isooctane reverse micelles with w = 10 is about 9.6 nm, hence the water pool diameter is about 7.2 nm.

$$D_h = 6.6 + 0.3w \tag{3.1}$$

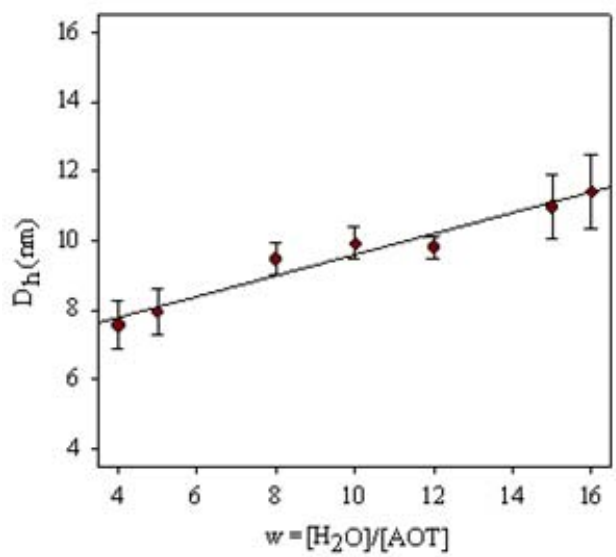

Figure 16: Hydrodynamic diameter measurements for water/AOT/isooctane reverse micelles.

3.3 Preparation of reverse micelles

A stock solution of AOT/isooctane at 0.5 M was prepared. Aqueous solutions of $KAuCl_4$ and K_2SO_3 were prepared at the concentrations shown in Table 3. The potassium sulfite solution was prepared inside a glove box under nitrogen atmosphere to avoid

oxidation of the sulfite. The molar concentration ratio of $[K_2SO_3]$ / $[KAuCl_4]$ = 3.4 was kept constant for all preparations in order to ensure the complete reduction of the metal salt.

Table 3: Experimental concentrations selected for the aqueous salt precursors.

Sample	**$[KAuCl_4]$ mM**	**$[K_2SO_3]$ mM**
Au1	38.00	129.49
Au2	57.55	194.24
Au3	76.74	258.99

We prepared two reverse micelle solutions, one of them containing the metal salt precursor and the other one the potassium sulfite. The preparation of these microemulsions involved the mixing of 10 ml of 0.5 M AOT in isooctane with 0.9 ml of aqueous stock solutions of $[Au^{+3}]$ or $[SO_3^{-2}]$ in order to obtain the desired value of *w*. The reverse micelle solution containing potassium sulfite was prepared inside a glove box under nitrogen atmosphere, because sulfite rapidly oxidizes when exposed to oxygen.

3.4 Gold nanoparticle synthesis

The synthesis of gold nanoparticles in reverse micelles with w = 10 was performed at a constant temperature of 25 ºC. The microemulsion prepared with $[SO_3^{-2}]$ was slowly added to the microemulsion prepared with $[Au^{+3}]$ under magnetic stirring. Because of the intermicellar exchange process between the reverse micelles, the reduction of ionic gold $[Au^{+3}]$ to atomic state $[Au^0]$ is achieved inside the water droplets according to the chemical reaction [50]

$$2Au^{+3} + 3SO_3^{-2} + 3H_2O \rightarrow 2Au^0 + 3SO_4^{-2} + 6H^+ . \quad (3.2)$$

The product of this reaction quickly changes color from transparent to a deep red or purple color depending on the concentrations of the aqueous salt precursors used. An illustration of this effect is shown in Figure 17.

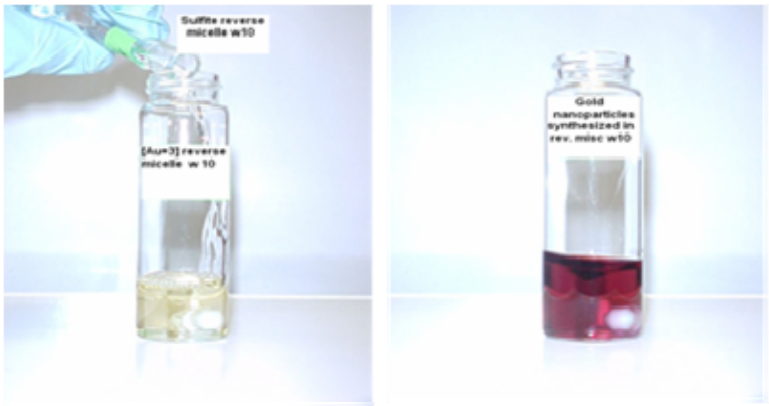

Figure17: Gold nanoparticles synthesized in reverse micelles with w = 10.

3.5 Gold colloids in aqueous media

Commercial gold colloids in aqueous media were purchased from Ted Pella Inc. Their sizes, coefficient of variations (CV), and roudness were characterized from TEM measurements. Gold colloids in aqueous media were stored at room temperature. The principal characteristics of these standards are summarized in Table 4.

3.6 Characterization

Extinction spectra of gold colloid standards in aqueous media and in reverse micelles with w = 10 were acquired using a Shimadzu UV-Vis 2401 spectrophotometer. Hydrodynamic diameters were measured by DLS. An SX.18MV Stopped Flow Reactor

(SFR) from Applied Photophysics Ltd. was used to follow the formation of gold nanoparticles in reverse micelles. The shape and nominal size of gold nanoparticles were determined using a ZEISS 922 Transmission Electron Microscope (TEM) operating at an accelerating voltage of 200 keV.

Table 4: Commercial gold colloids in aqueous media from Ted Pella Inc.

Nominal size (nm)	**particles per ml**	**Coefficient of variation**
5	5×10^{13}	<10%
10	5.7×10^{12}	<10%
15.2	1.4×10^{12}	<10%
20.3	7×10^{11}	<8%
30.7	2×10^{11}	<8%
40.3	9×10^{10}	<8%
52.6	4.5×10^{10}	<8%
59.4	2.6×10^{10}	<8%
81.1	1.1×10^{10}	<8%
100	5.6×10^{9}	<8%

4. RESULTS AND DISCUSSION

4.1 Extinction measurements

The sizes of the gold nanoparticles synthesized in reverse micelles were correlated to the optical signal of their plasmon resonance peak according to Mie theory. An extinction calibration curve was obtained from 200 to 1100 nm wavelength using commercial gold colloids of sizes ranging from 5 to 100 nm in aqueous media and in reverse micelles prepared with $w = 10$. Figures 18 and 19 show the extinction spectra obtained from these measurements.

In the aqueous samples the gold colloid volume fraction was less than 0.004%, whereas in the reverse micelle samples the gold colloid volume fraction was less than 0.0003%. Furthermore, the reported size distribution for the gold colloids was fairly narrow (the coefficient of variation was less than 10% according to the manufacturer, as shown in Table 4). These conditions lead us to believe that the extinction spectra in Figures 18 and 19 are representative of the optical behavior of a system of non-interacting particles with little polydispersity, hence we may analyze the results using Mie theory. To this end, the peak wavelength (λ_{max}) was correlated to the particle size. A red-shift was observed with increasing gold colloid size, as expected from Mie theory [5, 38].

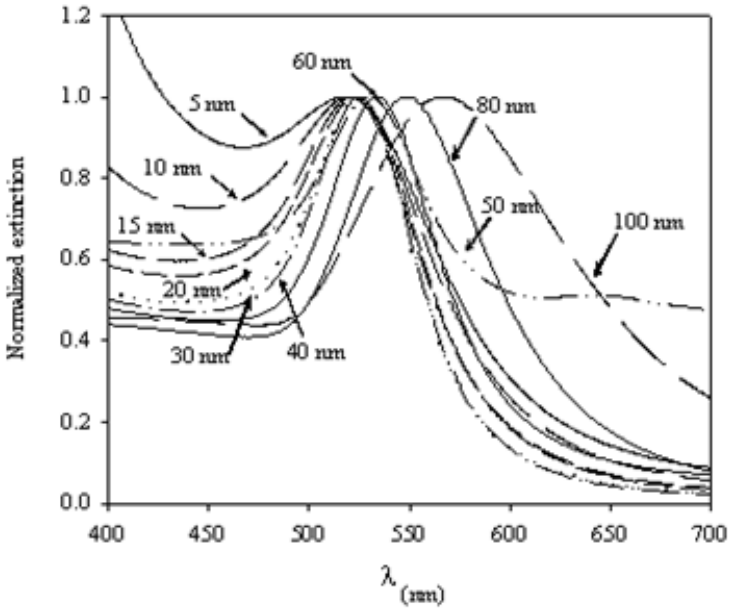

Figure 18: Extinction measurements of gold colloid standards in aqueous medium.

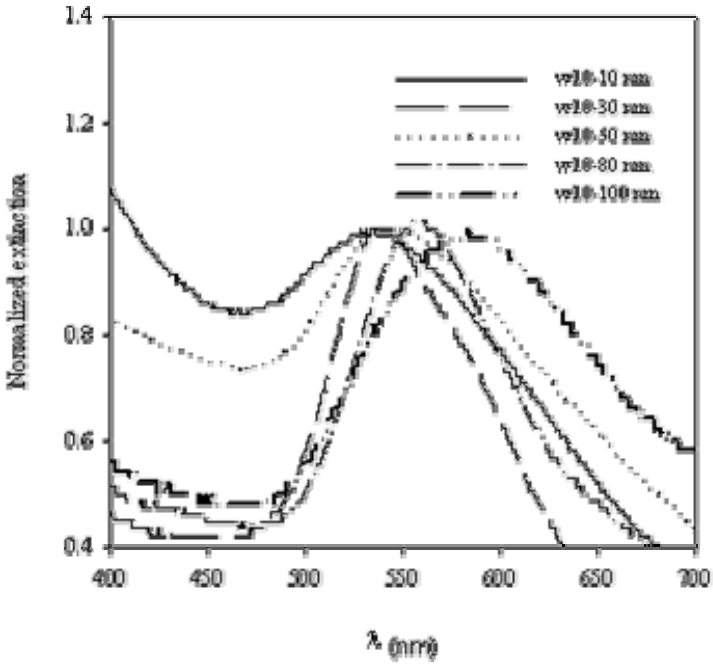

Figure 19: Extinction of gold colloid standards in AOT/water/isooctane reverse micelles with $w = 10$.

Figure 20 summarizes the results of correlating the peak wavelength (λ_{max}) to the particle size in both media, along with predictions based on Mie theory for three scenarious. First we considered gold nanoparticles suspended in aqueous media. Second we contemplated gold nanoparticles suspended in isooctane. Third we examined the possibility of having gold nanoparticles coated with an outer shell of 1.2 nm thickness corresponding to the AOT molecule; in this case, the core-shell extension of Mie theory was used [41, 42].

From Figure 20 it is observed that the third model had the best fit to the experimental extinction measurements of gold nanoparticles in reverse micelles. This observation encouraged the hypothesis that the particles are either inside the reverse micelles (for the smaller particles) or coated with a monolayer of surfactant. This model of core-shell structure could be supported by the observations reported by Capek [51], who have remarked that reverse micelles not only act as micro reactors for synthesis of metal nanoparticles, but also allow nanoparticle stabilization, because surfactant molecules could adsorb on the surface of the metal nanoparticle when it reaches the size of the water pool.

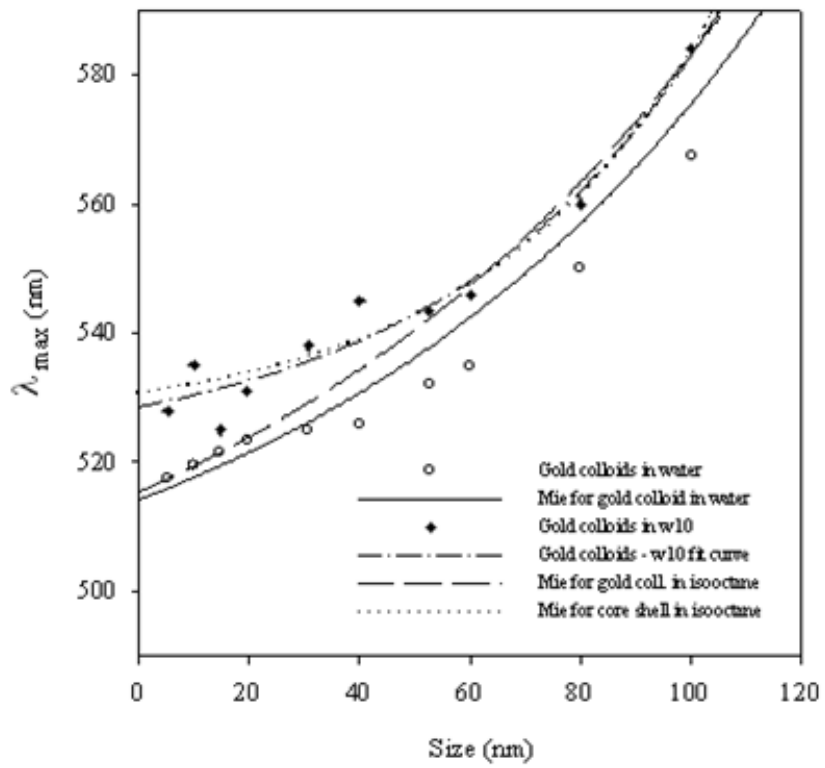

Figure 20: Peak wavelength correlation with particle size for gold nanoparticle in AOT/water/isooctane with $w = 10$.

4.2 Dynamic Light Scattering (DLS) measurements

In order to characterize the size and polydispersity of the gold nanoparticles synthesized, we performed an analysis of the diameters of commercial gold colloids in aqueous media and in reverse micelles with $w = 10$ through DLS measurements at 90° scattering angle; these samples were previously filtered with $0.2\,\mu m$ nylon membrane filters for the aqueous solutions and $0.1\,\mu m$ PTFE membrane filters for the organic media. Figure 21 shows a comparison between these measurements and the nominal size reported for the gold colloid standards in Table 4.

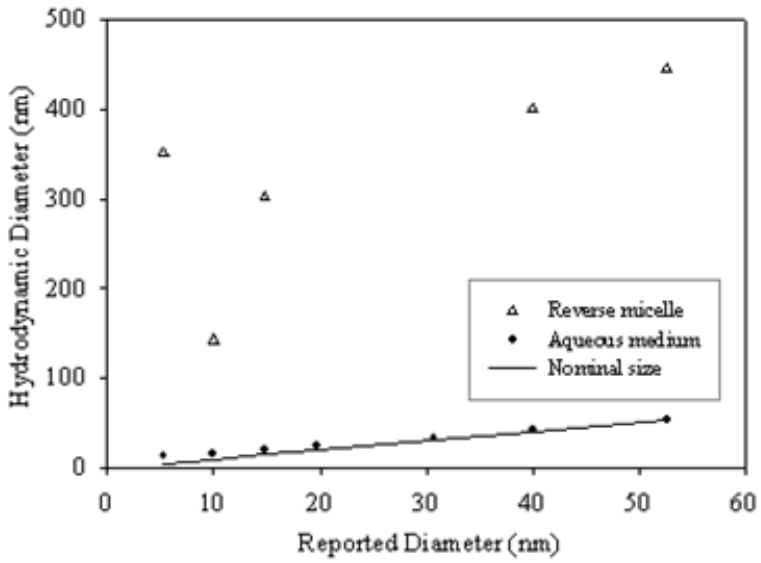

Figure 21: Comparison between nominal size of gold colloid standards and hydrodynamic diameter measured by DLS instrument. • gold colloid standards in aqueous medium, and Δ gold colloid standards in reverse micelles solution. The solid line represents exact correspondence between our measured hydrodynamic diameter and the value reported by the supplier.

Figure 21 shows that the hydrodynamic diameters (D_h) measured for gold colloids in aqueous media agree well with the nominal size reported by the supplier (determined by TEM). However, measurements in reverse micelle solutions indicated much larger hydrodynamic diameters and exhibited high polydispersity (>0.4). Wilcoxon and co-workers [48] made similar observations when using DLS to characterize gold nanoparticles synthesized in reverse micelles. They attributed these results to the metallic nature of gold colloids, which contribute to increasing the intensity of scattered light from micellar media. We agree with their observations, but also believe that the observed high values of D_h could be a result of agglomeration of the particles in the micelles. This motivated us to consider the stability of such systems from a theoretical perspective.

4.3 Particle-particle interaction in reverse micelles

We studied the agglomeration stability of gold nanoparticles inside reverse micelles by calculating the total interaction energy Φ_{total} between pairs of particles as a function of particle size. A soft sphere model [52] was used in which the reverse micelle was replaced by a gold nanoparticle with an adsorbed monolayer of AOT suspended in isooctane. In this way, the effect of water inside the reverse micelle was neglected as a first approximation. It is believed that after particle formation the water in the micelle mainly hydrates the surfactant head groups [53]. Here we present results for interacting pairs of equal diameter.

The total interaction energy Φ_{total} between two of our reverse micelles containing gold nanoparticles can be calculated from the sum of the interactions which govern the stability of the nanoparticles [24]. The van der Waals interaction Φ_{vdW} is the dominant attraction, and is dependent on the particle radius R, the center to center separation distance d, and the Hamaker constant A_{131}, which plays an important role in the description of the attraction energy between particles [9, 12]. Subscript 1 in the Hamaker constant refers to particles of the same material, separated by a continuous medium, represented through subscript 3. Under our conditions the Hamaker constant will always be positive and the van der Waals interaction is given by:

$$\Phi_{vdW} = -\frac{A_{131}}{6}\left[\frac{2R^2}{d^2-4R^2}+\frac{2R^2}{d^2}+\ln\left(\frac{d^2-4R^2}{d^2}\right)\right], \tag{4.1}$$

$$A_{131} = \left(\sqrt{A_{11}}-\sqrt{A_{33}}\right)^2. \tag{4.2}$$

In equation (4.1) the term A_{11} represents the gold-gold nanoparticle interaction, taken here as 45.3×10^{-20} J [54], and A_{33} corresponds to the solvent interaction, which for isooctane we take as 4.5×10^{-20} J [24]. These values for A_{11} and A_{33} were calculated using the Lifshitz theory for two identical materials interacting across a vacuum.

Another important effect that contributes to the total interaction energy is the repulsive forces due to overlapping of the surfactant tails covering the gold nanoparticles, and their interactions with the surrounding solvent molecules. These interactions can be modeled as an osmotic repulsion Φ_{osm} [12], which depends on various thermodynamic properties of the system, such as the solubility of the surfactant molecules in the organic solvent, and the reaction temperature [12, 52]

$$\Phi_{osm} = \frac{4\pi R k_B T}{\upsilon_{solv}} \phi^2 \left(\frac{1}{2} - \chi\right)\left(l - \frac{h}{2}\right)^2, \quad l < h < 2l . \tag{4.3}$$

Here k_B is Boltzmann's constant (1.38×10^{-23} J/K), υ_{solv} is the molecular volume of the isooctane, equivalent to 212.2 Å^3 [55], ϕ is the volume fraction occupied by the AOT molecule, χ is the Flory-Huggins interaction parameter, l is the chain length of the AOT, and h represents the particle-particle separation distance. The volume fraction and Flory-Huggins parameter may be calculated from:

$$\phi = 0.9\left[\frac{3R^2 l}{(R+l)^3 - R^3}\right], \tag{4.4}$$

$$\chi = \frac{\bar{v}_3}{R'T}(\delta_3 - \delta_2)^2, \tag{4.5}$$

$$h = d - 2R\,. \tag{4.6}$$

In equation (4.5), $\bar{v}_3$ represents the molar volume of the isooctane ($163.5\ \mathrm{cm^3/mol}$) [56], R' is the ideal gas constant, and δ_i are the Hildebrand solubility parameters, in which δ_3 corresponds to the isooctane solubility, which has a value of 15.4 $\mathrm{MPa^{0.5}}$ [56], and δ_2 is related to the AOT solubility, which when calculated according to group contribution methods (as shown in Appendix B), is equal to 12.26 $\mathrm{MPa^{0.5}}$ [57].

The total interaction is the sum of the van der Waals and osmotic contributions, which we calculate as a function of particle-particle separation distance and the size of the particles. One such interaction curve is shown in Figure 22 for particles of 6.4 nm diameter at $25^\circ\mathrm{C}$. A local minimum is observed between 2 and 3 nm separation distance. The presence of such local minima could lead to reversible flocculation of growing particles during synthesis. We therefore considered the change in interaction with increasing particle size and compared the depth of the local energy well to $-1.5\,k_B T$, for which we assume thermal energy would not prevent agglomeration [9, 12]. One such curve is shown in Figure 23 for particles of 6-22 nm in diameter. A local minimum is always observed between 2-3 nm, corresponding to same overlapping of the surfactant tails. The depth of the minimum increases with increasing diameter and our analysis would indicate that particles larger than about 8 nm diameter should reversibly coagulate. The results of this analysis serve to explain our observed large hydrodynamic diameters for the gold colloid standards in reverse micelles (Figure 21).

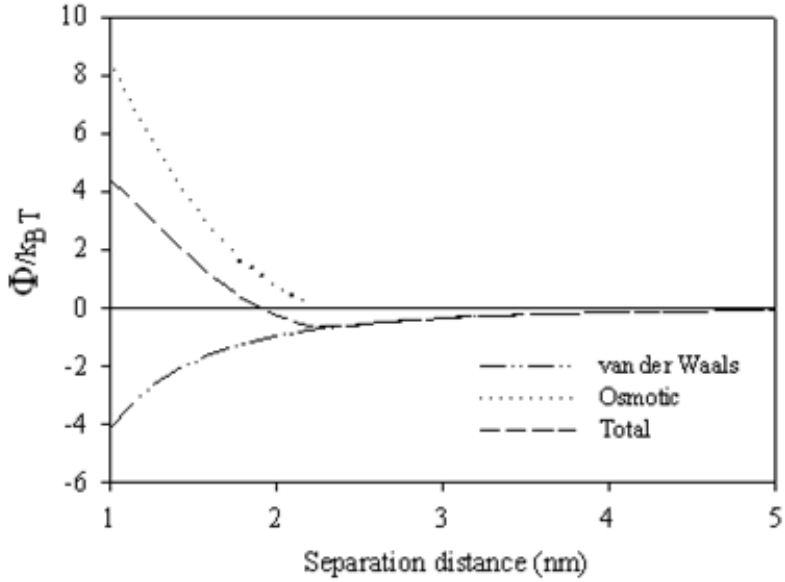

Figure 22: Contributions to the total interaction energy for gold nanoparticles coated with a layer of AOT and immersed in isooctane at 25 °C . Particle diameter is 6.4 nm

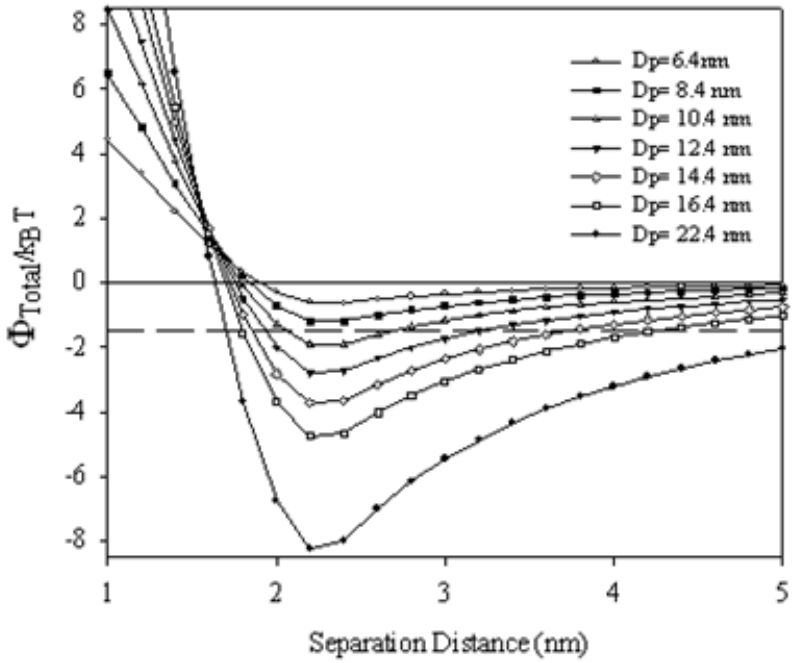

Figure 23: Total interaction energy as a function of separation distance for various particle diameters.

4.4 Transmission Electron Microscope (TEM) measurements

We used a ZEISS 922 TEM with an accelerating voltage of 200 keV and a magnification of 160000x, to determine the shape and size of gold nanoparticles synthesized with w = 10 at different concentrations. A drop from each synthesis was deposited on a copper grid with a carbon support film, and dried at room temperature. Some results of these measurements are shown in Figure 24, from which we observe that gold nanoparticles exhibit a spherical form, with diameters of 8 to 10 nm. Though this could be an artifact of sample preparation, most particles were observed as part of clusters, with lower density of particles. Larger particles were not observed.

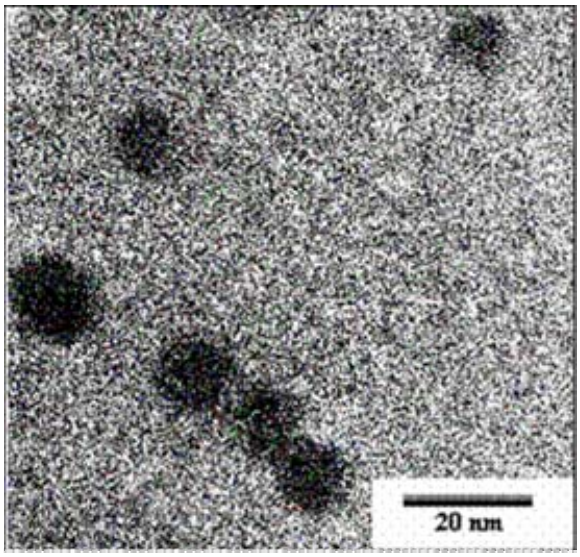

Figure 24: TEM of gold nanoparticles synthesized with Au3 concentration in w =10 reverse micelles.

Arcoleo and co-workers [58] synthesized gold nanoparticles in the system water/AOT/n-heptane and used Atomic Force Microscopy (AFM) to study particle size and agglomeration when deposited in atomically flat silicon wafers. They found evidence of clusters with sizes of the order of 200-400 nm, and individual particles with sizes

roughly 30-100 nm. Because of the technique and conditions used in their study, these measurements (particularly those of the individual particles) are admittedly rough estimates. Our TEM measurements are in qualitative agreement yet show the individual particle size to be smaller than that estimated by Arcoleo and co-workers. Still, our findings agree with their proposition that a surfactant layer forms around the larger particles preventing their further growth.

4.5 Growth and agglomeration kinetics

We used an SX.18MV Stopped Flow Reactor (SFR) with a 256 element photodiode linear array to obtain complete UV-Vis spectra as a function of time and follow the growth and agglomeration kinetics of gold nanoparticles synthesized in the water/AOT/isooctane reverse micelles with w = 10. This equipment uses a pneumatic drive of 125 psi N_2 to rapidly mix two microemulsions prepared with [Au^{+3}] and [SO_3^{-2}] respectively, eliminating mass transfer limitations. The reaction is illuminated by a 150 W ozone free Xenon arc lamp to measure absorption changes as a function of time in the range of 200 to 730 nm.

We observed the gold nanoparticle synthesis process for a period of 262 seconds. Figure 25 shows a characteristic trace of absorption spectra obtained from these measurements. It is seen that the peak wavelength red-shifts with time during the process. Porta and co-workers [59], have synthesized gold nanoparticles in reverse micelle solutions from the reduction of auric sodium tetrachloride ($NaAuCl_4$), and

hydrazine. They observed a red shift from 500 up to 535 nm with increasing particle size, in agreement with our results.

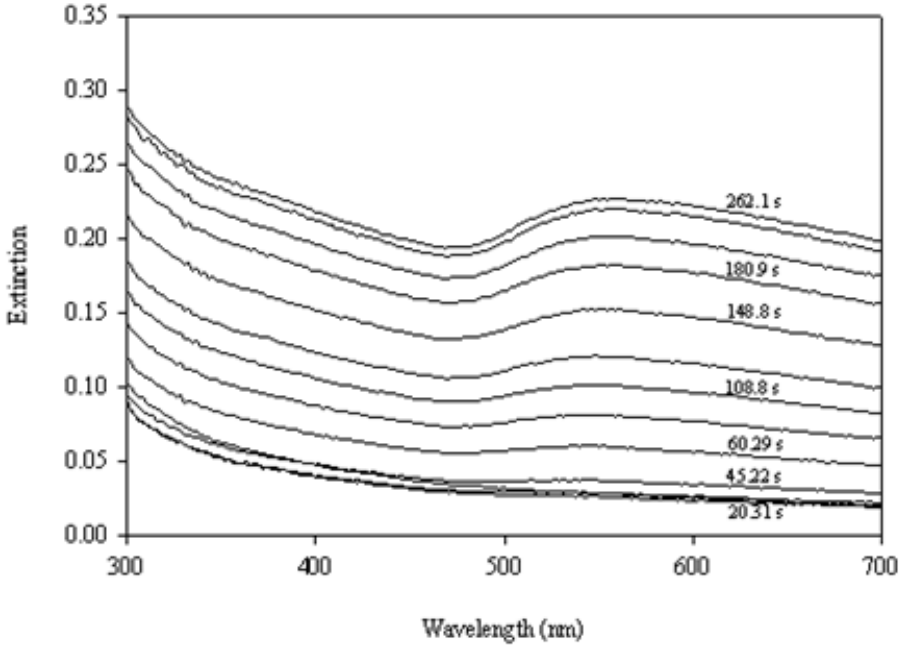

Figure 25: Time correlated extinction spectra of gold nanoparticles synthesized in reverse micelles with w = 10 for Au1 sample concentration ($KAuCl_4$ [38 mM], K_2SO_3[129.49 mM])

Figures 26 a. to 26 c. show the displacement of the maximum extinction wavelength (λ_{max}) during the reaction. Red shifts from 535 to 570 nm are observed. Using the results of Figure 20, the observed maximum extinction wavelength could be correlated to a time evolution of effective particle size, which would change from 25 to 85 nm. Such large particle sizes would indicate that our reverse micelles do not control the final particle size (recall that the water pool diameter had been estimated to be approximately 7.2 nm). Furthermore, our interaction energy analysis indicated that particles above 8 nm in diameter should agglomerate; this would affect the absorption spectrum of the sample and invalidate the use of Mie theory to correlate peak wavelength to particle size.

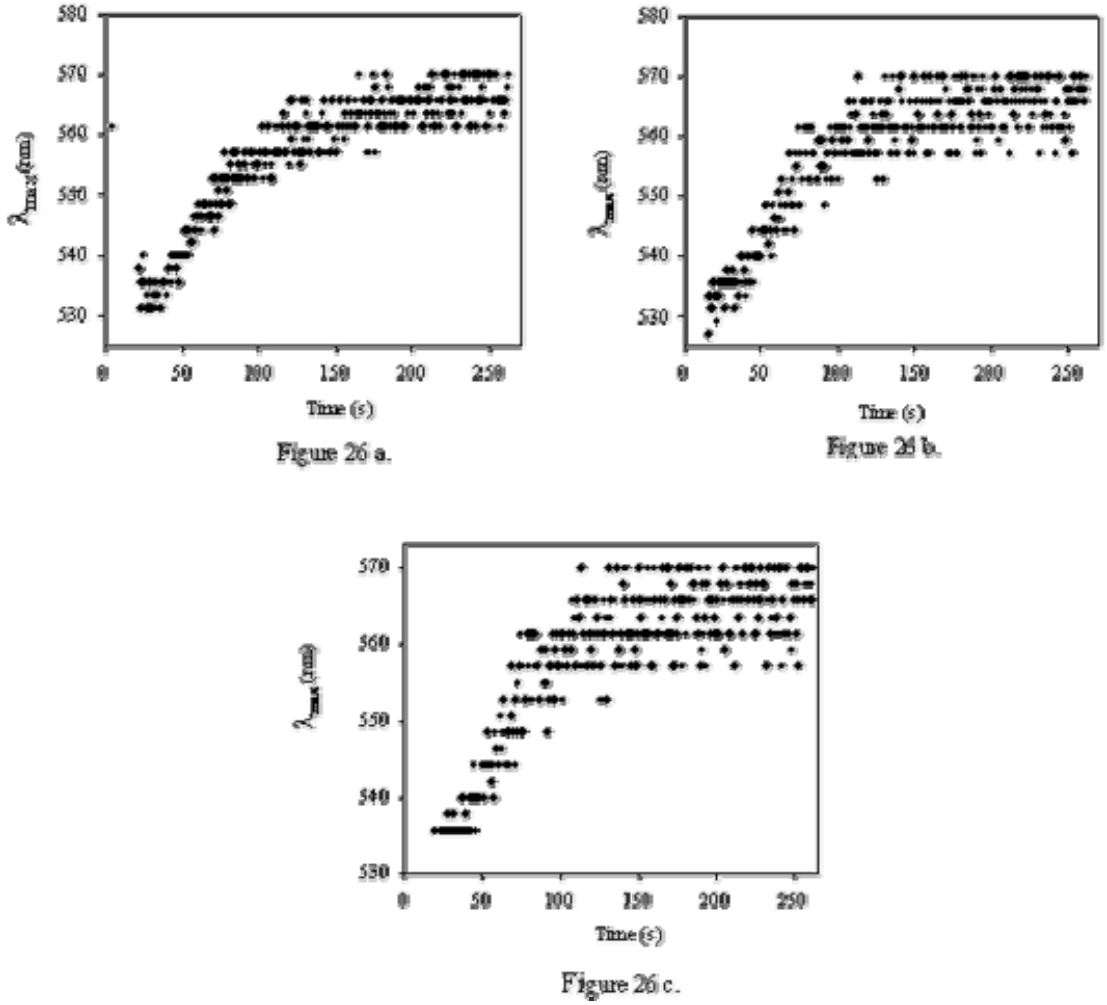

Figure 26: Change in the peak extinction wavelength for gold nanoparticles synthesized in reverse micelles with w = 10 for: a) Au1: $KAuCl_4$ [38 mM], K_2SO_3[129.49 mM], b) Au2: $KAuCl_4$ [57.55 mM], K_2SO_3[194.24 mM] and c) Au3: $KAuCl_4$ [76.74 mM], K_2SO_3[258.99 mM]

Finally, TEM measurements showed gold nanoparticles of 8-10 nm in diameter, and evidence of cluster formation. Such clusters would result in multiple scattering and splitting of the plasmon resonance band into two peaks due to interaction between particles. Also, particle size polydispersity during the synthesis process could result in an apparent red shift or the appearance of a long-wavelength tail [60]. When two gold nanoparticles approach at relatively short distances an electrodynamic interaction

phenomenon is expected [61]. This interaction results in the displacement of the plasmon resonance signal. Rechberger and co-workers [61] have analyzed the electrodynamic interactions that occur in a pair of gold nanoparticles of equal size as a function of distance along the centers of the particles. They observed a remarkable red shift of the surface plasmon extinction peak with decreasing interparticles distance, which could be misconstrued to correspond to a single gold nanoparticle of larger size.

The effect of multiple scattering can be analyzed from more elaborate optical theories. Fonseca and co-workers [62] have studied the extinction due to fractal colloidal aggregates of metallic particles, modeling the effect of multiple scattering through Maxwell-Garnett and Bruggeman theories, which consider the contribution of light scattering from a particle and its neighbors through effective medium models [37]. From their analysis, they obtained a good representation of the optical properties of colloidal aggregates whose size increases through aggregation. An analysis such as this could be applied to translate our measurements to information on aggregate growth as a function of time.

5. CONCLUSIONS

A core-shell Mie model provided the best fit to measurements of peak absorption wavelength as a function of particle size for gold colloids in reverse micelles formed in the system water/AOT/isooctane. This suggested that particles are either contained in the water pool of the micelles (for smaller particles) or coated by a layer of AOT surfactant.

DLS measurements of the hydrodynamic diameters of the particles in reverse micelles indicated, however, a considerable degree of agglomeration. This observation was verified through an interaction energy analysis considering van der Waals attraction between particles and osmotic repulsion due to the adsorbed surfactant. The analysis indicated the presence of a local energy minimum greater than $-1.5\,k_B T$ for particles of 8.4 nm diameter, suggesting that reversible flocculation may occur for particles of that size and larger.

These observations would indicate that during synthesis of gold nanoparticles in reverse micelles of the system water/AOT/Isooctane, particles would grow through intermicellar exchange to a size of about 8 nm in diameter and then agglomerate. Upon agglomeration, further growth would be hindered as the intermicellar exchange is slowed or prevented. This hypothesis is confirmed through TEM measurements showing particles of 8 to 10 nm in diameter forming small clusters. Larger particles were not observed. Time resolved UV-Vis extinction spectra were obtained and the peak absorption wavelength was extracted as a function of time. Because of agglomeration and multiple scattering, Mie theory cannot be used to translate these results to particle size as a function of time, as has been previously done for gold nanoparticle synthesis in aqueous media. Rather, our results could be interpreted using multiple scattering theories, such as that by Fonseca and co-workers [62] to obtain a measure of aggregate size as a function of time, thereby obtaining information on aggregation kinetics during synthesis.

6. RECOMMENDATIONS

The synthesis of gold nanoparticles in reverse micelles offers an interesting research field, which must be focused on to satisfy the demand of tailoring metal nanoparticles with well defined shape and size distribution for industrial applications [7, 46].

For this reason, our work can serve as a point of reference, because it explores the synthesis of gold nanoparticles from a complete study that encompassed optical theories, spectroscopy and microscopy techniques, and light scattering study supported by a theoretical analysis of the total interaction energy between nanoparticles, which give us a better perspective to understand the stability of the synthesized gold nanoparticles. It is important to remark that this work also provides a complete literature review which allowed us to establish a solid base for results comparison.

In order to improve the results obtained in this work, several recommendations could be taken into account; among them the use of cosurfactants like alcohols or poly-ethylene ethers [17, 25], which affect the interface rigidity of reverse micelles allowing a better control on the rate of exchange of materials between them. The addition of a cosurfactant could enhance the repulsion forces observed in the particle-particle interaction analysis (section 4.3), avoiding reversible coagulation of the gold nanoparticles, and hence growth kinetics, could be observed from SFR measurements (section 4.5).

Another important factor that could be considered for future work is the analysis of particle-particle interaction between reverse micelles of different sizes, which could to verify our theoretical analysis of the coagulation of gold nanoparticles.

Furthermore, the effect of multiple scattering could be analyzed from Maxwell-Garnett or Bruggeman optical theories, in which are considered the contribution of light scattering from a particle and its neighbors through effective medium models [37]. This would provide a relationship between colloidal aggregate growth as a function of reaction time and optical properties of the suspension.

Experimental measurements of the attraction interaction (Φ_{vdW}) between reverse micelles containing gold nanoparticles could enhance the theoretical results obtained from the total interaction analysis (Φ_{Total}). These measurements could be carried out with an Atomic Force Microscope (AFM) [58, 63, 64], which measure the deflection of a cantilever (or sharp tip) as a function of sample displacement. With these measurements, we could estimate the attraction force between a commercial gold coated tip and a flat gold substrate submerged in an AOT/isooctane solution, as shown in Figure 27. This could provide a test for the Hamaker constants used in our theoretical calculations.

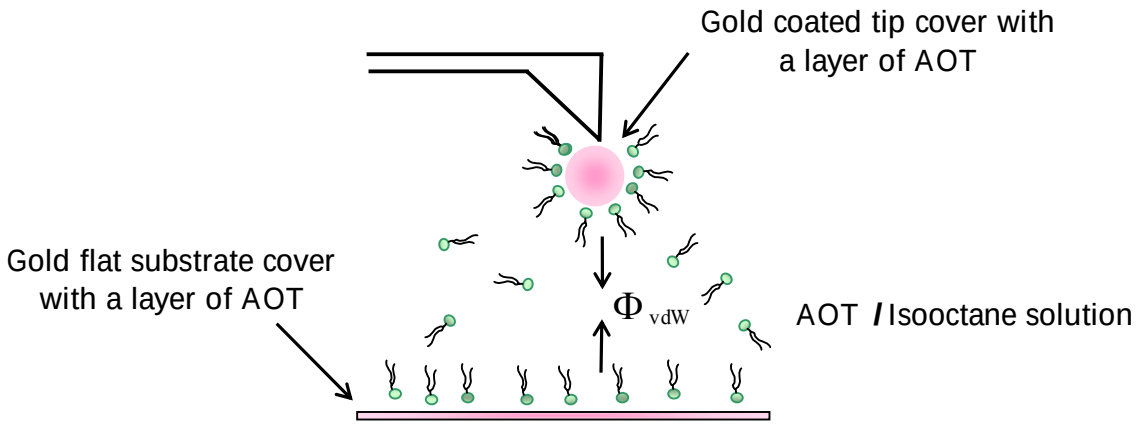

Figure 27: Illustration of the measurement of forces between a gold coated tip and a gold flat substrate in AOT/Isooctane solution using an AFM.

Some issues could be expected from these AFM measurements; one of them is the AOT surface layer on the coated tip and the flat substrate, because the AOT has a packing parameter larger than unity. Moreover, surface roughness would be an important factor, it could affect the measurements of van der Waals forces at nanometric distances between the gold coated tip and the flat gold substrate [65, 66].

Finally, it would be interesting to analyze the effect of pH on the size of the reverse micelle's water pool as the formation of gold nanoparticles through reduction could lead to changes in pH. It is important to remark that these changes in pH could affect the kinetics study of nanoparticle formation in reverse micelle structure [67]

APPENDIX A.

Collision parameters for reverse micelles with *w* = 10

A.1 Collision rate (Z)

Defining the following parameters [12]:

Z: magnitude of the collision rate (number of collision between reverse micelles)

h: distance of separation

J: flux of reverse micelles.

According to Fick's law

$$J = -D\frac{dN}{dh}, \tag{A.1}$$

where *N* is the total number of reverse micelles per volume of solution, and *D* is the diffusion coefficient, which is expressed in terms of the Stokes-Einstein relation:

$$D = \frac{k_B T}{6\pi\eta R_h}, \tag{A.2}$$

in which R_h is the hydrodynamic radius of the reverse micelles.

The Diffusion of the particle in steady state is given by:

$$\frac{\partial N}{\partial t} = D\frac{1}{h^2}\frac{\partial}{\partial h}\left(\frac{h^2 \partial N}{\partial h}\right) = 0. \tag{A.3}$$

Integrating equation (A.3):

$$N_{(h)} = \frac{-B}{h} + C, \tag{A.4}$$

in equation (4) B and C are the integration constants. Applying the boundary conditions:

$$\begin{aligned} &h \to \infty \text{ when } N_{(h)} = N_{bulk} = C, \text{ and} \\ &h \to R_h \text{ when } N_{(h)} = 0, \text{ then } B = N_{bulk} R_h \end{aligned} \tag{A.5}$$

Taking equation (5) in equation (4):

$$N_{(h)} = \frac{-N_{Bulk} R_h}{h} + N_{Bulk}\,, \tag{A.6}$$

Taking the derivative with respect to h

$$\frac{dN_{(h)}}{dh} = \frac{N_{Bulk} R_h}{h^2}\ . \tag{A.7}$$

An expression for the flux at the contact point (when h approaches to R_h) could be obtained taking equation (7) in equation (1):

$$J\Big|_{h=R_h} = \frac{-DN_{Bulk} R_h}{R_h^2} = \frac{-DN_{Bulk}}{R_h}\ . \tag{A.8}$$

The collision rate Z is defined as the product of flux and contact area, and is given by:

$$Z = 16\pi D N_{Bulk} R_h\,. \tag{A.9}$$

Taking equation (A.2) in equation (A.9):

$$Z = \frac{8k_B T}{3\eta} N_{Bulk}\,. \tag{A.10}$$

Here k_B is Boltzmann's constant (1.38×10^{-23} J/K), T is the temperature of the microemulsion system (298.15 K), and η is the viscosity of the bulk solvent isooctane, equivalent to 0.51 cp [55].

From DLS measurements (section 3.2) the hydrodynamic radius (R_h) of a reverse micelles prepared with w = 10 was determined to be equal to 4.8 nm. Assuming spherical shape, the volume of each reverse micelle is about $463.23\ \text{nm}^3$; and the volume of the micellar solution is given by:

$$V_{solution} = V_{H2O} + (V_{AOT} + V_{Isooctane}) . \tag{A.11}$$

In section 3.3 was detailed the preparation of reverse micelles as the mixed of 10 ml of 0.5 M AOT in isooctane with 0.9 ml of aqueous stock solutions; from this data and equation (11) could be determined the bulk concentration of micelles per volume of solution.

$$N_{Bulk} = \frac{V_{aqueous}}{V_{solution} * V_{micelle}} = 0.0001782\ \text{micelle/nm}^3 . \tag{A.12}$$

Taking the value of N_{Bulk} in equation (10), is found a rate of collision (Z) equal to 3911.39 s^{-1}

A.2 Time between collisions (t)

The time between collisions (t) is defined as the reciprocal of the collision rate:

$$t = \frac{1}{Z} = 25.5\ \mu\text{s} , \tag{A.13}$$

which means that the collisions between reverse micelles is too fast allowing micellar coalescence and the exchange of their water contents.

APPENDIX B.

Calculation of the solubility parameters of AOT in Isooctane

B.1 AOT Solubility (δ_2):

The solubility parameter of AOT (δ_2) is estimated using a group contribution method usually applied to polymer solutions; in which a molar attraction constant (G) is defined for each chemical group of the surfactant tail [52]. Table B-1 shows representative group molar attraction constants based on intermolecular forces [57].

Table B-1:Group molar attraction constant. Adapted from [57].

Number	Group	G [(cal cm^3)$^{0.5}$ mol $^{-1}$]
1	CH_3 —	147.3
2	—CH_2—	131.5
3	>CH —	85.99

The solubility parameter (δ_2) is related to the group molar attraction constant (G) by

$$\delta_2 = \frac{d\sum G}{M}, \tag{B.1}$$

where d is the density of AOT equal to 1.13 g/ml [56], and M is the molecular weight of the group contribution.

From the AOT structure displayed in Figure 1-6, we can distinguish the characteristic groups shown in table B-1, where group number 2 has three contributions. The molecular weight of all group contributions is equal to 113 g/mol, and then applying equation (B.1), we obtain a solubility parameter for AOT equal to:

$$\delta_2 = 5.99\left(\frac{\text{cal}}{\text{cm}^3}\right)^{0.5} = 12.26\left(\text{MPa}\right)^{0.5} \tag{B.2}$$

B.2 Flory Huggins parameter (χ):

After determining the solubility parameter of AOT (δ_2) we can determine the Flory Huggins parameter (χ) through equation (4.5), substituting the molar volume of the isooctane ($\bar{v}_3$), and its solubility parameter (δ_3), both related in section 4.3.

$$\chi = 0.27 \tag{B.3}$$

The Flory Huggins parameter is related to the solvent interactions between AOT tails and the molecules of the organic solvent (isooctane); we can observe a good solvent region because $\chi < 0.5$.

APPENDIX C.

Volumetric fraction (ϕ_{vol}) of gold colloid standards in aqueous media and in water/AOT/isooctane solution.

Table C1. Volumetric fraction (ϕ_{vol}) of gold colloid standards in aqueous media and in water/AOT/isooctane solution

Nominal size (nm)	Particles/ml	C.V	ϕ_{vol} in aqueous media (%)	ϕ_{vol} in reverse micelles (%)
5	5×10^{13}	<8%	0.0032	0.00026
10	5.7×10^{12}	<10%	0.0029	0.00023
15.2	1.4×10^{12}	<10%	0.003	0.00022
20.3	7×10^{11}	<8%	0.003	0.00024
30.7	2×10^{11}	<8%	0.003	0.00024
40.3	9×10^{10}	<8%	0.003	0.00024
52.6	4.5×10^{10}	<8%	0.0034	0.00028
59.4	2.6×10^{10}	<8%	0.0028	0.00023
81.1	1.1×10^{10}	<8%	0.003	0.00023
100	5.6×10^{9}	<8%	0.0029	0.00023

APPENDIX D.

Calculation of the theoretical yield and volumetric fraction of gold nanoparticles synthesized in reverse micelles with *w* = 10

D.1 Theoretical yield

We could obtain the theoretical yield of gold nanoparticles synthesized from the experimental concentrations of the aqueous salt precursors displayed on Table 3 (section 3.3).

For Au1 sample:

$$0.038\frac{\text{mol}}{\text{L}}\text{Au}^{+3}\times 9\times 10^{-4}\,\text{L} = 3.42\times 10^{-5}\,\text{mol Au}^{+3}$$

From equation (3.2) we observed a 1:1 molar ratio of Au^{+3} to Au^{0}:

$$3.42\times 10^{-5}\,\text{mol Au}^{+3} = 3.42\times 10^{-5}\,\text{mol Au}^{0}$$

The theoretical yield is given by:

$$3.42\times 10^{-5}\,\text{mol Au}^{0}\times 196.96\frac{\text{g}}{\text{mol Au}^{0}} = 0.00673\,\text{g Au}^{0}$$

Table D.1 displays the theoretical yield calculated for Au1, Au2, and Au3 sample concentrations.

Table D.1: Theoretical yield obtained from experimental concentrations of the aqueous salt precursors.

Sample	Theoretical yield (g)
Au1	0.00673
Au2	0.01020
Au3	0.01360

D.2 Volumetric fractions (ϕ_{vol})

Taking gold density equivalent to 19.3 g/ml, and a total volume of micellar solution of 20 ml, we could obtain the volumetric fraction of gold nanoparticles synthesized in reverse micelles with w = 10 by using the theoretical yield displayed on table D.1. These results are summarized in Table D.2

Table D.2: Volumetric fraction (ϕ_{vol}) of gold nanoparticles synthesized in reverse micelles with w = 10.

Sample	**ϕ_{vol} (%)**
Au1	0.0017
Au2	0.0026
Au3	0.0035

APPENDIX E.

Change in the peak extinction wavelength during reaction time

Figures E-1 to E-3 show the displacement of the maximum extinction wavelength (λ_{max}) during the synthesis of gold nanoparticles in reverse micelles with w = 10 at different concentrations of the aqueous salt precursors.

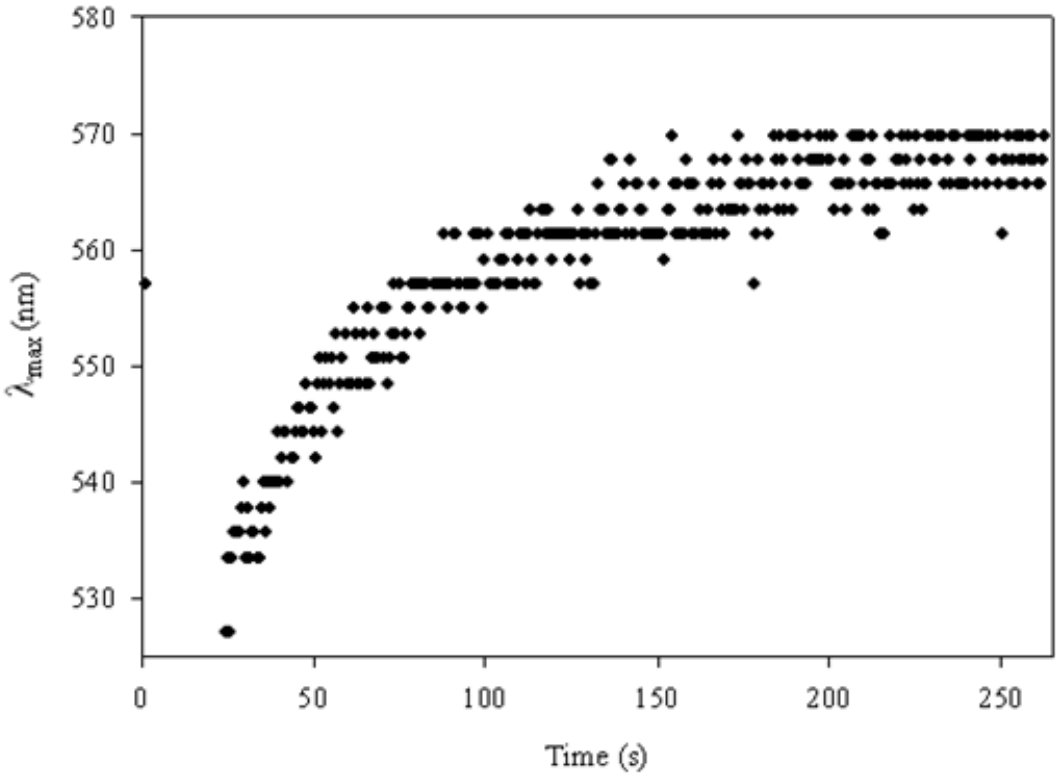

Figure E-1: Au1 concentration up to 262 s Au1: $KAuCl_4$ [38 mM], K_2SO_3 [129.49 mM].

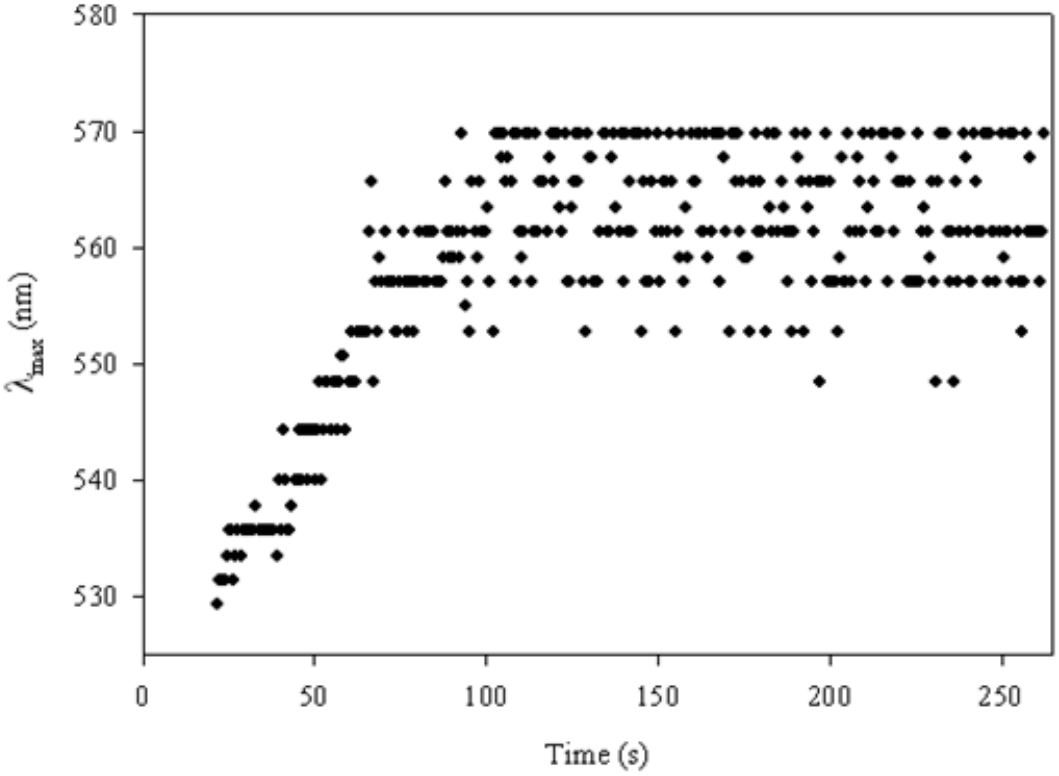

Figure E-2: Au2 concentration up to 262 s. Au1: $KAuCl_4$ [57.55 mM], K_2SO_3 [194.24 mM].

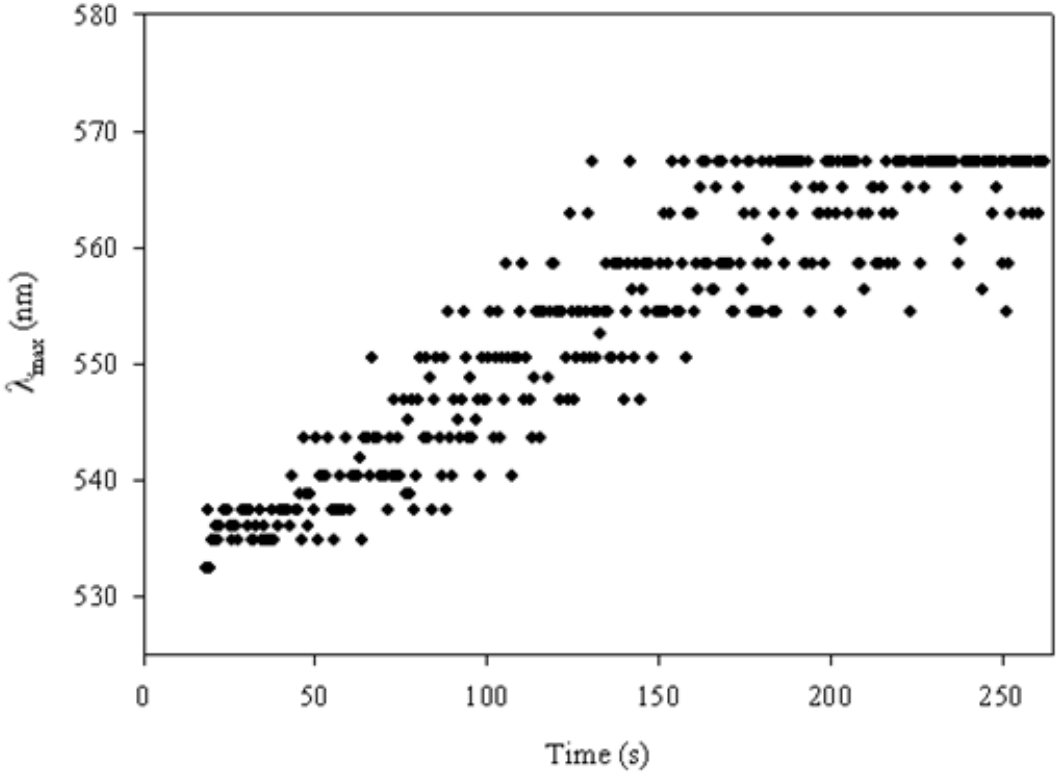

Figure E-3: Au3 concentration up to 262 s. Au1: $KAuCl_4$ [76.74 mM], K_2SO_3 [258.99mM].

BIBLIOGRAPHY

[1] R. Feynman, "Annual meeting of the American Physical Society," California Institute of Technology, 1959.

[2] D. Feldheim and C. Foss, *Metal nanoparticles: Synthesis, characterization and applications*. New York, 2002.

[3] J. Hainfield and R. Powell, "New frontiers in gold labeling," *Journal of Histochemistry and Cytochemistry*, vol. 48, pp. 471-479, 2000.

[4] B. Palpant, B. Prével, J. Lermé, M. Treilleux, and J. Vialle, "Optical properties of gold clusters in the size range 2-4 nm," *Physical Review B*, vol. 57, pp. 1963-1970, 1998.

[5] U. Kreibig and M. Vollmer, *Optical properties of metal clusters*. Germany, 1995.

[6] V. Roldughin, "Quantum-size colloid metal system," *Russian Chemical Reviews*, vol. 69, pp. 821-843, 2000.

[7] S. Penn, L. He, and M. Natan, "Nanoparticles for Bioanalysis," *Current Opinion in Biotechnology*, vol. 7, pp. 1-7, 2003.

[8] R. Rich and D. Myszka, "Advances in surface plasmon resonance biosensor analysis," *Current Opinion in Biotechnology*, vol. 11, pp. 54-61, 2000.

[9] D. F. Evans and H. Wennerstrom, *The Colloidal Domain: Where Physics, Chemistry, Bioogy, and Technology meet.*, Second ed. Canada, 1999.

[10] J. Israelachvili, D. Mitchell, and B. Ninham, "Theory of self-assembly of hydrocarbon amphiphiles into micelles and bilayers," *Journal of the Chemical Society Faraday Transactions II.*, vol. 72, pp. 1525-1568, 1975.

[11] D. Langevin, "Structure of reverse micelles," in *Structure and Reactivity in Reverse Micelles*, Elsevier, Ed. New York, 1989, pp. 13-43.

[12] P. Hiemenz and R. Rajagopalan, *Principles of Colloid and Surface Chemistry*, Third ed, 1997.

[13] M. Kotlarchyk, J. Huang, and S. Chen, "Structure of AOT reversed micelles determined by Small Angle Neutron Scattering," *Journal of Physical Chemistry*, vol. 89, pp. 4382-4386, 1985.

[14] C. Tanford, "Micelle shape and size," *Journal of Physical Chemistry*, vol. 76, pp. 3020-3024, 1972.

[15] G. Cassin, J. Badiali, and M. Pileni, "AOT reverse micelles: depletion model," *Journal of Physical Chemistry*, vol. 99, pp. 12941-12946, 1995.

[16] M. Pileni, "Fabrication and properties of nanosized materials material made by using coloidal assemblies as templates," *Crystal Research Technology*, vol. 33, pp. 1155-1168, 1998.

[17] T. H. L. Nazário., J. Crespo, "Nonionic cosurfactants in AOT reversed micelles: effect on percolation size and solubilization site," *Langmuir*, vol. 12, pp. 6326-6335, 1996.

[18] D. Stigter and K. Mysels, "Tracer electrophoresis II: The mobility of the micelle of Sodium lauryl sulfate and its interpretation in terms of zeta potential and charge," *Journal of Physical Chemistry*, vol. 59, pp. 45-51, 1955.

[19] M. D'Angelo, D. Fioretto, and G. Onori, "Interparticle interactions in water in oil microemulsions: dielectric and IR investigations," *Physical Review E*, vol. 58, pp. 7657-7663, 1998.

[20] P. Fletcher, A. Howe, and B. Robinson, "The kinetics of solubilizate exchange between water droplets of a water in oil microemulsions," *Journal of the Chemical Society Faraday Transactions I.*, vol. 83, pp. 985-1000, 1987.

[21] P. Alexandridis, J. Holzwarth, and T. Hatton, "Interfacial dynamics of water in oil microemulsion droplets: Determination of the bending modulus using Iodine Laser Temperature Jump," *Langmuir*, vol. 9, pp. 2045-2052, 1993.

[22] H. Bohidar and M. Behboudnia, "Characterization of reverse micelles by Dynamic Light Scattering," *Colloids and Surfaces A*, vol. 178, pp. 313-323, 2001.

[23] J. Lang and A. Jada, "Structure and dynamics of water in oil droplets stabilized by Sodium Bis(2-ethylhexyl) Sulfosuccinate," *Journal of Physical Chemistry*, vol. 92, pp. 1946-1953, 1988.

[24] J. Israelachvili, *Intermolecular & Surface Forces*, Second ed. San Diego, California, 1991.

[25] J. M. D. liu., H. Cheng., Z. Zhao, "Investigation on the conductivity and microstructure of AOT/non-ionic surfactants/water/n-heptane mixed reverse micelles," *Colloids and Surfaces A*, vol. 135, pp. 157-164, 1998.

[26] M. Sahyun, "Total luminescence spectroscopy in a reverse micellar system," *Journal of Physical Chemistry*, vol. 92, pp. 6028-6032, 1988.

[27] M. Pileni, "Reverse micelles as microreactors," *Journal of Physical Chemistry*, vol. 97, pp. 6961-6973, 1993.

[28] M. Pileni, T. Zemb, and C. Petit, "Solubilization by reverse micelles: solute localization and structure perturbation," *Chemical Physics Letters*, vol. 118, pp. 414-420, 1985.

[29] D. R. S. Brunetti., M. Bellocq., G. Fourche., P. Bothore, "Micellar interactions in water in oil microemulsions light scattering determinations of the second virial coefficient," *Journal of Physical Chemistry*, vol. 87, pp. 1028-1034, 1982.

[30] J. Eastoe, W. Young, and B. Robinson, "Scattering studies of microemulsions in low density alkanes," *Journal of the Chemical Society Faraday Transactions.*, vol. 86, pp. 2883-2889, 1990.

[31] M. Zulauf and H. Eicke, "Inverted micelles and microemulsions in the ternary system water/Aerosol-OT/Isooctane as studied by photon correlation spectroscopy," *Journal of Physical Chemistry*, vol. 83, pp. 480-486, 1979.

[32] A. Howe, C. Toprakcioglu, J. Dore, and B. Robinson, "Small Angle Neutron Scattering studies of microemulsions stabilized by Aerosol-OT," *Journal of Chemical Society Faraday Transactions I.*, vol. 82, pp. 2411-2422, 1986.

[33] E. Kaler, J. Billman, J. Fulton, and R. Smith, "A Small Angle Neutron Scattering study of the intermicellar interactions in microemulsions of AOT, water and near critical propane," *Journal of Physical Chemistry*, vol. 95, pp. 458-462, 1991.

[34] J. Nicholoson and J. Clarke, "Photon correlation techniques in the investigations of water in oil microemulsions," in *Surfactants in Solution*. New York: Plenum Press, 1984, pp. 1663-1674.

[35] J. W. S. Liu., M. Save., S. Arnes, "Synthesis of pH responsive shell cross-linked micelles and their use as nanoreactors for the preparation of gold nanoparticles," *Langmuir*, vol. 18, pp. 8350-8357, 2002.

[36] H. Kwok, *Electronic Materials*. New York, 1997.

[37] C. Bohren and D. Huffman, *Absorption and Scattering of Light by Small Particles*. New York, 1998.

[38] I. Sosa, C. Noguez, and R. Barrera, "Optical properties of metal nanoparticles with arbitrary shapes," *Journal of Physical Chemistry. B*, vol. 107, pp. 6269-6275, 2003.

[39] J. Schmitt, P. Machtle, D. Eck, H. Mohwald, and C. Helm, "Preparation and optical properties of colloidal gold monolayers," *Langmuir*, vol. 15, pp. 3256-3266, 1999.

[40] P. Johnson and R. Christy, "Optical constant of the nobel metals," *Physical Review B*, vol. 6, pp. 4370-4379, 1972.

[41] R. Averitt, S. Westcott, and N. Halas, "Linear optical properties of gold nanoshells," *Journal of Optical Society of America. B*, vol. 16, pp. 1824-1832, 1999.

[42] R. Averitt, D. Sarkar, and N. Halas, "Plasmon resonance shifts of Au-coated Au_2S nanoshells: insight into multicomponent nanoparticle growth," *Physical Review Letters*, vol. 78, pp. 4217-4220, 1997.

[43] R. Baer, D. Neuhauser, and S. Weiss, "Enhanced absorption induced by a metallic nanoshell," *Nano Letters*, vol. 4, pp. 85-88, 2004.

[44] L. Murillo, O. Viera, E. Vicuña, J. Briano, M. Castro, Y. Ishikawa, R. Irizarry, and L. Solá, "Growth kinetics of gold nanoparticles," presented at Computational Nanoscience and Nanotechnology, www.cr.org, 2002.

[45] E. Vicuña, O. Viera, J. Briano, M. Castro, Y. Ishikawa, R. Irizarry, and L. Solá, "Polydisperse mixture of gold nanoparticles," presented at Computational Nanoscience and Nanotechnology, www.cr.org, 2003.

[46] C. Chiang, "Controlled growth of gold nanoparticles in AOT/$C_{12}E_4$/Isooctane mixed reverse mielles," *Journal of Colloid and Interface Science*, vol. 239, pp. 334-341, 2001.

[47] J. Lin, W. Zhou, and C. O'Connor, "Formation of ordered arrays of gold nanoparticles from CTAB reverse micelles," *Materials Letters*, vol. 49, pp. 282-287, 2001.

[48] J. Wilcoxon, R. Williamson, and R. Baughman, "Optical properties of gold colloids formed in inverse micelles," *Journal of Chemical Physics*, vol. 98, pp. 9933-9950, 1993.

[49] C. Fengxi, X. Guo-Quin, and T. A. Hor, "Preparation and assembly of colloidal gold nanoparticles in CTAB stabilized reverse microemulsions.," *Materials Letters*, vol. 4325, pp. 1-5, 2003.

[50] J. Bailor, H. Eméleus, R. Nyholm, and T. Dickerson, *Comprehensive Inorganic Chemistry*. Oxford: Pergamon Press, 1973.

[51] I. Capek, "Preparation of metal nanoparticles in water-in-oil (w/o) microemulsions.," *Advances in Colloid and Interface Science*, vol. 110, pp. 49-74, 2004.

[52] C. Kitchens, M. Chandler, and C. Roberts, "Solvent effects on the growth and steric stabilization of copper metallic nanoparticles in AOT reverse micelle systems," *Journal of Physical Chemistry*, vol. 107, pp. 11331-11338, 2003.

[53] P. Shah, J. Holmes, J. K, and B. Korgel, "Size-selective dispersion of dodecanethiol-coated nanocrystals in liquid and supercritical ethane by density tuning," *Journal of Physical Chemistry B*, vol. 106, pp. 2545-2550, 2002.

[54] D. Bargeman and F. V. V. Vader, "Van der Waals forces between immersed particles," *Journal of Electroanalytical Chemistry and Interfacial Electrochemistry*, vol. 37, pp. 45-52, 1972.

[55] V. Sedivec and J. Flek, *Handbook of Analysis of Organic Solvents*. London England, 1976.

[56] D. Peck, R. Schechter, and K. Jhonston, "Unified classical and molecular thermodynamic theory of spherical water in oil microemulsions," *Journal of Physical Chemistry*, vol. 95, pp. 9541-9549, 1991.

[57] M. P. Stevens, *Polymer Chemistry: An Introduction*, Third Edition ed. New York, 1999.

[58] V. Arcoleo and V. T. Liveri, "AFM investigation of gold nanoparticles synthesized in water/AOT/n-heptane microemulsions," *Chemical Physics Letters*, vol. 258, pp. 223-227, 1996.

[59] F. Porta, L. Prati, M. Rossi, and G. Scarí, "Syntheis of Au(0) nanoparticles from W/O microemulsions," *Colloids and Surfaces A*, pp. 43-48, 2002.

[60] D. Goia and E. Matijevic, "Preparation of monodispersed metal particles," *New Journal of Chemistry*, pp. 1203-1215, 1998.

[61] W. Rechberger, A. Hohenau, A. Leitner, J. Kreen, B. Lamprecht, and F. Aussenegg, "Optical properties of two interacting gold nanoparticles," *Optics Communications*, vol. 220, pp. 137-141, 2003.

[62] L. Fonseca, M. Gomez, and L. Cruz, "Calculation of the aggregation and electrodynamic effects in granular systems," *Physica A*, vol. 207, pp. 123-130, 1994.

[63] W. Ducker, T. Senden, and R. Pashley, "Direct measurement of colloidal forces using an Atomic Force Microscope," *Nature*, vol. 353, pp. 239-241, 1991.

[64] W. Ducker and T. Senden, "Measurement of forces in liquids using a Force Microscope," *Langmuir*, vol. 8, pp. 1831-1836, 1992.

[65] G. Toikka, R. Hayes, and J. Ralston, "Surface forces between spherical ZnS particles in aqueous electrolyte," *Langmuir*, vol. 12, pp. 3783-3788, 1996.

[66] M. Gotzinger and W. Peukert, "Dispersive forces of particle-surface interactions: direct AFM measurements and modelling," *Powder Technology*, vol. 130, pp. 102-109, 2003.

[67] P. Walde, Q. Mao, R. Bru, P. Luigi, and R. Kuboi, "pH artifacts in reverse micellar enzymology: a warning," *Pure and Applied Chemistry*, vol. 64, pp. 1771-1775, 1992.